

Structured H_∞ -control of infinite dimensional systems

P. Apkarian^{1*}, D. Noll²

Abstract

We develop a novel frequency-based H_∞ -control method for a large class of infinite-dimensional Linear-Time-Invariant systems in transfer function form. We use a non-smooth trust-region method to compute arbitrarily structured locally optimal H_∞ -controllers for a frequency sampled approximation of the underlying infinite-dimensional H_∞ -problem in such a way that exponential stability in closed-loop is guaranteed, and the optimal value of the approximation captures the value of the infinite-dimensional problem within a prior tolerance level. We demonstrate the versatility and practicality of our method on a variety of infinite-dimensional H_∞ -synthesis problems, including distributed and boundary control of PDEs, control of dead time and delay systems, and using a rich testing set.

Keywords

H_∞ -control — infinite dimensional systems — frequency domain design — Nyquist stability — winding numbers — stability certificate — performance certificate

¹ Control System Department, ONERA, 2, av. Ed. Belin, 31055, Toulouse, France

² Institut de Mathématiques de Toulouse, 118 route de Narbonne F-31062, Toulouse, France

*Corresponding author: P. Apkarian & D. Noll

Contents

	Introduction	1
1	Winding numbers, Nyquist stability	3
2	Sampled Nyquist test with certificate	5
3	Optimization method	6
4	Sampling for synthesis with certificate	7
5	Illustrating remarks and examples	9
6	Application in process control	10
7	Delay systems	12
8	Comparison with convex-concave procedure	14
9	More exhaustive testing	15
10	Conclusion	15
	References	15

Introduction

In this work we use a frequency-based H_∞ -method to control infinite-dimensional LTI-systems $G(s)$. After embedding $G(s)$ as usual in a plant $P(s)$ and setting up performance and robustness channels $T_{wz}(P, K)$, we address the infinite-dimensional H_∞ -optimization problem

$$\begin{aligned} & \text{minimize} && \max_{\omega \in [0, \infty]} \bar{\sigma}(T_{wz}(P(j\omega), K(j\omega))) \\ & \text{subject to} && K \text{ stabilizes } G \text{ exponentially} \\ & && K \in \mathcal{K} \end{aligned} \quad (1)$$

where optimization is over a class \mathcal{K} of structured finite rank control laws. Our strategy is to choose frequency samples $G(j\omega_v)$ of $G(s)$ in such a way that the solution $K^* \in \mathcal{K}$ of the approximate H_∞ program

$$\begin{aligned} & \text{minimize} && \max_{v=1, \dots, N} \bar{\sigma}(T_{wz}(P(j\omega_v), K(j\omega_v))) \\ & \text{subject to} && K \text{ stabilizes } G \text{ exponentially} \\ & && K \in \mathcal{K} \end{aligned} \quad (2)$$

guarantees closed-loop stability for $G(s)$, and assures that the value of (2) differs only by a fixed tolerance ϑ from the true value of (1). Sampling in the frequency domain becomes necessary since the objective of (1) is semi-infinite, non-smooth, and non-convex, and not directly amenable to efficient computation.

The difficulty in program (1) is further aggravated by the fact that controllers $K \in \mathcal{K}$ have to be *structured* in the sense of [1]. Structured controllers or control architectures are preferred by practitioners and include classics like PIDs, lead-lag and notch filters, polynomial matrix fractions, reduced fixed-order controllers, but also observer-based controllers, distributed control architectures interconnecting other structured elements, decentralized control, and much else. A general way to model structure uses state-space in the form

$$K(s) : \begin{cases} \dot{x}_K &= A_K(\mathbf{x})x_K + B_K(\mathbf{x})y \\ u &= C_K(\mathbf{x})x_K + D_K(\mathbf{x})y. \end{cases} \quad (3)$$

where $A_K(\cdot)$, $B_K(\cdot)$, ... are smooth matrix-valued functions of a tunable parameter vector $\mathbf{x} \in \mathbb{R}^n$, but our method applies also to infinite-dimensional controller structures $K(\mathbf{x})$

as long as they are parametrized by a finite-dimensional vector $\mathbf{x} \in \mathbb{R}^n$ of tunable parameters. With this restriction programs (1), (2) fall within the class of so-called semi-infinite optimization problems [2].

For systems given in state-space we obtain the transfer function $G(s)$ directly from the infinite dimensional system. We then discretize $G(j\omega_v)$ on the low-dimensional level of the input-output map, where sampling is best adapted to the truly relevant dynamics of the system. In consequence, versions of (2) with essentially no loss over (1) typically require only a very moderate number N of samples, rarely exceeding a couple of hundred nodes, so that (2) is solved in seconds to minutes. Pre-computing samples $G(j\omega_v)$ may turn out more time-consuming, but since we perform it offline, it does not impede the optimization or the plant-modeling phase. Our method is also suited for systems provided from start in frequency sampled form (2), or for systems given directly by their transfer function.

In order to justify our approach theoretically, we have to clarify the following issues:

- (a) How to sample the return difference $\det(I + GK)$ so that exponential stability in closed loop is guaranteed.
- (b) How to sample the transfer function $G(s)$ so that the approximate value of (2) is within a fixed tolerance ϑ of the true value of (1).
- (c) How to solve the non-smooth optimization program (2) algorithmically.

To address the stability issue (a) we implement an infinite-dimensional Nyquist test, which is effective as soon as stability of the closed-loop systems is *spectrum-determined*. This applies for instance to delay and dead-time systems, to boundary and distributed control for parabolic PDEs, or to control of hyperbolic PDEs of one space dimension. In contrast, control of hyperbolic PDEs of several space dimensions requires a case-by-case analysis.

Analysis of the stability issue (a) reveals the surprising fact that most of the time only a very limited number of frequency samples $G(j\omega_v)$ are needed to obtain the correct winding number. On the other hand, the sampling grid for stability Ω_{nyq} depends on the candidate controllers $K \in \mathcal{K}$, and therefore needs updating during optimization.

A second important aspect of question (a) is how stability can be built into a mathematical programming constraint in order to maintain it during optimization (2). This cannot be based on the Nyquist test, which is discrete in nature, and we propose a stability barrier function based on the modulus margin of the closed-loop system.

Appropriate frequency sampling to assure performance (b) benefits from the fact [3] that for a fixed control law $K \in \mathcal{K}$ the frequency response, even when exhibiting sharp primary and secondary peaks, is twice continuously differentiable as a function of frequency in the neighborhood of those peaks. This improves the order of the approximation and

leads to an efficient sampling method. Non-smoothness typically occurs at anti-resonances, but as those are irrelevant for a good approximation of the frequency maximum in (1), the number of nodes needed for a good approximations is moderate and rarely exceeds a couple of hundred.

Optimization (c) is based on the non-smooth trust-region method of [4], which was already successfully applied to computation of the structured distance to instability in [5]. For the solution of program (2) specific features of the method are exploited to gain speed, on which we comment in section 3. A technical difficulty arises from the fact that the sampling grid for performance Ω_{opt} , unlike for stability, cannot be adapted to the candidate controllers $K \in \mathcal{K}$ during optimization, as this would change program (2). Posterior verification of the optimal controller $K^* \in \mathcal{K}$ obtained on the current Ω_{opt} is therefore necessary, and may require occasional restarts on a refined optimization grid. The overall procedure including these re-starts given in algorithm 3 is still speedy and converges within seconds to minutes.

A side aspect of our approach is that it allows to avoid the use of system reduction and identification techniques and to stay as close as possible to the infinite-dimensional program (1), confining discretization to the level of the transfer function.

Even though our primary interest here lies in situations where the transfer function $G(s)$ is available analytically, or numerically at arbitrary frequencies, program (2) also contributes novel aspects in cases where from start only a frequency sampled version $G(j\omega_v)$ is available for synthesis, with no recourse to further missing values $G(j\omega)$. Our present techniques may then still be applied to reduce program (2) from the original fine sampling Ω_{fine} to a manageable size Ω_{opt} for optimization, with stability and performance certificates then valid under the proviso that the information stored in the initial finest available sample Ω_{fine} is sufficiently rich.

There is a plethora of literature on controller design based on frequency-domain data, and we just cite a few. Pioneering work is the semi-infinite programming technique proposed by Polak [6], and the Quantitative Feedback Theory (QFT) of [7] is in this class. More recently, various optimization-based techniques have been studied. Linear programming or convex optimization is proposed for specific controller structures in [8, 9, 10]. A more general convex-concave procedure (CCP) is used in [11] to design PIDs, and in [12] is extended to linearly parameterized MIMO PIDs. In the same vein, the arXiv paper [13] applies CCP to synthesize MIMO fraction-of-polynomial controllers. These specific controller structures allow design specifications in the form of convex differences. Linearizing concave terms then yields LMI subproblems, which are solved sequentially to determine locally optimal controllers. Note a general analysis of CCP together with variations and extensions is discussed in [14].

Nyquist stability for infinite dimensional systems has a long history and is discussed in [15], an axiomatic approach being [16]. In [17] extensions to trace class operators are pro-

posed. The link between input-output and exponential stability is discussed in [18].

The structure of the paper is as follows. Section 1 discusses theoretical and practical aspects of the Nyquist test and its use to enforce closed-loop stability in (2). Grid selection for the Nyquist test is presented in section 2. Section 3 presents our optimization method for (2), grid selection for optimization Ω_{opt} being discussed in section 4. Sections 6, 7 discuss control of crystallization and dead-time processes. A numerical evaluation of our method using the test bench [19], along with several PDE studies, is presented in Section 9.

Notation

Our notation is covered by [20]. A standing assumption is that the system transfer function is of the form $G(s) = C(sI - A)^{-1}B + D$, where A is the infinitesimal generator of a strongly continuous semi-group on a Hilbert space [20, 21], with finite rank input and output space $U \simeq \mathbb{R}^p$ and $Y \simeq \mathbb{R}^m$. This means B, D are bounded, while C could be closed unbounded and satisfies $D(A) \subset D(C)$. As a consequence of the finite rank assumption, $G(s)$ is meromorphic, see [22]. Controllers $K \in \mathcal{K}$ have similar state-space realizations with input and output spaces Y, U .

1. Winding numbers, Nyquist stability

In this section we discuss how the closed-loop stability constraint in optimization program (2) is implemented. As our approach is frequency based, it is natural to use the Nyquist stability criterion. We introduce $F(s) = I + G(s)K(s)$ and $f(s) = \det F(s)$, and also

$$\mathcal{F}(s) = \begin{bmatrix} I & K(s) \\ -G(s) & I \end{bmatrix}.$$

We define the number n_p of open-loop rhp poles as the number of rhp poles of \mathcal{F} . We need the following hypotheses:

- (i) G and K are proper.
- (ii) $f(s) = \det(I + G(s)K(s))$ has only finitely many poles and no zeros on $j\mathbb{R}$.
- (iii) The limit of $f(s) = \det(I + G(s)K(s))$ as $s \rightarrow \infty$ on $\overline{\mathbb{C}}^+$ exists and differs from 0.
- (iv) The state-space realization of $G(s)$ is exponentially stabilizable and detectable.
- (v) Candidate controllers $K \in \mathcal{K}$ have exponentially stabilizable and detectable state-space realizations.

Let h be holomorphic on a domain containing $\overline{\mathbb{C}}^+$ such that $h(s) \neq 0$ on \mathbb{C}^+ , $\lim_{s \rightarrow \infty} h(s) = 1$ on $\overline{\mathbb{C}}^+$, and such that h has a zero of order p at 0 or $\pm j\omega$ precisely when $f(s) = \det(I + G(s)K(s))$ has a pole of order p at 0 or $\pm j\omega$. Let $\tilde{f} = fh$. (If f has no poles on $j\mathbb{R}$, then $h = 1$). We call $\{\tilde{f}(j\omega) : \omega \in \mathbb{R} \cup \{\infty\}\}$ the modified infinite Nyquist curve.

Theorem 1. Let conditions (i)–(v) be satisfied. Suppose the modified infinite Nyquist curve $\{\tilde{f}(j\omega) : \omega \in \mathbb{R} \cup \{\infty\}\}$ winds n_p times around the origin in the clockwise sense, i.e.

$$\frac{1}{2\pi} \int_{-\infty}^{\infty} \frac{\tilde{f}'(j\omega)}{\tilde{f}(j\omega)} d\omega = n_p. \quad (4)$$

Then the closed-loop system is exponentially stable.

Proof. 1) Since B has finite rank and (A, B) is exponentially stabilizable, it satisfies the spectrum decomposition assumption at 0, see [20, p. 233 and p. 71]. Hence H may be decomposed as $H = H_- \oplus H_+$, where $H_\pm = P_\pm(H)$ for spectral projectors P_-, P_+ with $P_- + P_+ = I$ such that, on putting $A_\pm = A|_{H_\pm}$, $B_\pm = P_\pm \circ B$, $C_\pm = C \circ P_\pm$, such that with the coordinates $x = (x_-, x_+) = (P_-x, P_+x)$, the system (A, B, C, D) becomes

$$A = \begin{bmatrix} A_- & 0 \\ 0 & A_+ \end{bmatrix}, B = \begin{bmatrix} B_- \\ B_+ \end{bmatrix}, C = [C_- \ C_+], \quad (5)$$

with (A_-, B_-, C_-) exponentially stable, (A_+, B_+, C_+, D) finite dimensional and jointly stabilizable and detectable. For $G(s)$ we get a decomposition $G(s) = G_-(s) + G_+(s)$ with $G_-(s) = C_-(sI - A_-)^{-1}B_-$, $G_+(s) = C_+(sI - A_+)^{-1}B_+ + D$.

In consequence G_- is holomorphic on an open domain containing $\overline{\mathbb{C}}^+$, while G_+ has left and right coprime factorizations over \mathbf{H}_∞ , which can be extended meromorphically on an open domain containing $\overline{\mathbb{C}}^+$. By Lemma 2 the same is true for G . Similar factorizations are obtained for K .

2) Now since G, K have left coprime factorizations by part 1), so does \mathcal{F} . Indeed, suppose $G = M^{-1}N$ and $K = m^{-1}n$ are left coprime, then so is

$$\begin{bmatrix} I & K \\ -G & I \end{bmatrix} = \begin{bmatrix} m^{-1} & 0 \\ 0 & M^{-1} \end{bmatrix} \begin{bmatrix} m & n \\ -N & M \end{bmatrix}.$$

Call these matrices \mathcal{M} and \mathcal{N} , then $\mathcal{F} = \mathcal{M}^{-1}\mathcal{N}$, and $\det \mathcal{F} = \det \mathcal{N} / \det \mathcal{M}$. In particular, n_p is the number of rhp zeros of $\det(\mathcal{M})$.

3) Observe that $f = \det(I + GK)$ on any curve avoiding the finitely many rhp poles of G and K . Indeed, Schur complement gives

$$\begin{bmatrix} I & K \\ -G & I \end{bmatrix} = \begin{bmatrix} I & 0 \\ -G & I \end{bmatrix} \begin{bmatrix} I & K \\ 0 & I + GK \end{bmatrix}$$

hence for every s which is neither a rhp-pole of G nor of K we have $f(s) = \det(I + G(s)K(s)) = \det[I, K(s); -G(s), I] = \det \mathcal{F}(s)$.

4) Since G, K are proper by (i), they have only finitely many rhp poles. For $\varepsilon > 0$ let D_ε be a standard finite Nyquist D-contour with ε -half circle indentations into the right half plane at the finitely many poles of f on $j\mathbb{R}$. Suppose D is large enough and ε is small enough so that D_ε contains the n_p rhp poles of \mathcal{F} in its interior.

Now by the argument principle the index satisfies

$$\text{ind}(f \circ D_\varepsilon, 0) = n_z^\varepsilon - n_p,$$

where n_z^ε and n_p are the number of zeros and poles of f inside D_ε . Clearly f and $\tilde{f} = fh$ have the same number of zeros and poles inside D_ε , hence

$$\text{ind}(\tilde{f} \circ D_\varepsilon, 0) = n_z^\varepsilon - n_p.$$

But note that \tilde{f} is meromorphic on \mathbb{C}^+ and holomorphic on a domain containing $j\mathbb{R}$, as the poles of f on $j\mathbb{R}$ have been removed through h , so that in particular $\text{ind}(\tilde{f} \circ D, 0)$ is defined, where D is now the usual finite Nyquist contour obtained from D_ε by letting $\varepsilon \rightarrow 0$. That means

$$\text{ind}(fh \circ D, 0) = n_z^D - n_p,$$

where n_z^D is the number of zeros of fh , hence of f , inside the D -contour. Since $\lim_{s \rightarrow \infty} f(s) \neq 0$, we have $\lim_{s \rightarrow \infty} f(s)h(s) \neq 0$ on $\overline{\mathbb{C}^+}$, and then we may pass to the limit $\tilde{f}(D) \rightarrow \tilde{f}(j\mathbb{R})$ in the D -contour to obtain

$$\frac{1}{2\pi} \int_{-\infty}^{\infty} \frac{\tilde{f}(j\omega)}{\tilde{f}(j\omega)} d\omega = n_z - n_p,$$

where n_z is the number of zeros of fh , hence of f , on \mathbb{C}^+ . Using (4), we deduce that $n_z = 0$. Since \mathcal{M}, \mathcal{N} are coprime, we have derived that $\det \mathcal{N}(s) \neq 0$ on \mathbb{C}^+ .

5) Since \mathcal{N} is holomorphic on \mathbb{C}^+ and invertible, \mathcal{N}^{-1} is now also holomorphic on \mathbb{C}^+ , hence $\mathcal{F}^{-1} = \mathcal{N}^{-1}\mathcal{M}$ is holomorphic. But $\mathcal{F}^{-1} = \mathcal{T}$, where \mathcal{T} is the closed-loop transfer function

$$\mathcal{T} = \begin{bmatrix} I - K(I + GK)^{-1}G & K(I + GK)^{-1} \\ (I + GK)^{-1}G & (I + GK)^{-1} \end{bmatrix}, \quad (6)$$

so we have proved that \mathcal{T} is holomorphic on \mathbb{C}^+ .

We argue that $\mathcal{T} \in \mathbf{H}_\infty$. This follows from the fact that any of the four closed-loop transfer functions G_{cl} occurring in \mathcal{T} is proper, i.e. satisfies $\overline{\sigma}(G_{cl}(s)) \leq M$ for some $M > 0$, $\rho > 0$, and all s in $\{s \in \mathbb{C}^+ : |s| \geq \rho\}$. For $G_{cl} = (I + GK)^{-1}$ this follows from condition (iii), for terms containing K , G we invoke (i). This proves $\mathcal{T} \in \mathbf{H}_\infty$.

6) Suppose (A_K, B_K, C_K, D_K) is an exponentially stabilizable and detectable state-space realization of K . Then $\mathcal{T}(s)$ has the state space realization

$$\begin{bmatrix} I & D_K \\ -D & I \end{bmatrix}^{-1} \left\{ \begin{bmatrix} I & D_K \\ -D & I \end{bmatrix} - \begin{bmatrix} 0 & C_K \\ -C & 0 \end{bmatrix} (sI - A_{cl})^{-1} \right. \\ \left. + \begin{bmatrix} B & 0 \\ 0 & B_K \end{bmatrix} \right\} \begin{bmatrix} I & D_K \\ -D & I \end{bmatrix}^{-1},$$

where $[I, D_K; -D, I]$ is invertible by (iii) and

$$A_{cl} = \begin{bmatrix} A & 0 \\ 0 & A_K \end{bmatrix} - \begin{bmatrix} B & 0 \\ 0 & B_K \end{bmatrix} \begin{bmatrix} I & D_K \\ -D & I \end{bmatrix}^{-1} \begin{bmatrix} 0 & C_K \\ -C & 0 \end{bmatrix}.$$

Since $\mathcal{T} \in \mathbf{H}_\infty$, we also have

$$\begin{bmatrix} 0 & C_K \\ -C & 0 \end{bmatrix} (sI - A_{cl})^{-1} \begin{bmatrix} B & 0 \\ 0 & B_K \end{bmatrix} \in \mathbf{H}_\infty.$$

Now since (A, B, C) , (A_K, B_K, C_K) are jointly stabilizable and detectable, we deduce that

$$\left(A_{cl}, \begin{bmatrix} B & 0 \\ 0 & B_K \end{bmatrix}, \begin{bmatrix} 0 & C_K \\ -C & 0 \end{bmatrix} \right) \quad (7)$$

is jointly stabilizable and detectable. But now the result follows with Lemma 1, which we apply to (7). \square

Lemma 1. Suppose (A, B, C) is exponentially stabilizable and detectable with generator A on a Hilbert space H , and suppose $G(s) = C(sI - A)^{-1}B \in \mathbf{H}_\infty$. If B is bounded and $D(A) \subset D(C)$, then A generates an exponentially stable C_0 -semigroup.

Proof. By exponential stabilizability and detectability there exist bounded $K \in \mathcal{L}(H, U)$ and $L \in \mathcal{L}(Y, H)$ such that $A + BK$ and $A + LC$ generate exponentially stable semigroups. We have $\overline{\mathbb{C}^+} \subset \rho(A)$, and for $s \in \rho(A)$ we may write

$$\begin{aligned} (sI - A)^{-1} &= (sI - A - LC)^{-1}LG(s)K(sI - A - BK)^{-1} \\ &\quad + (sI - A - LC)^{-1}(sI - A - LC)(sI - A - BK)^{-1} \\ &\quad - (sI - A - LC)^{-1}BK(sI - A - BK)^{-1}. \end{aligned}$$

Since the resolvents $(sI - A - LC)^{-1}$ and $(sI - A - BK)^{-1}$ are uniformly bounded on \mathbb{C}^+ , and since by assumption

$$\sup_{s \in \mathbb{C}^+} \overline{\sigma}(G(s)) < \infty,$$

the first term on the right is bounded. The third term on the right is also bounded, because BK is bounded. As for the second term on the right, we clearly have $(sI - A - LC)^{-1}(sI - A - LC) = I$ on the domain of $sI - A - LC$. It is therefore enough to assure that the domain of $sI - A - LC$ contains the range of $(sI - A - BK)^{-1}$. But $D(sI - A - LC) = D(A)$ due to the hypothesis $D(A) \subset D(C)$, and on the other hand, the range of $(sI - A - BK)^{-1}$ equals the domain of $sI - A - BK$, hence the domain of $A + BK$, and since BK is bounded, this coincides with $D(A)$, so we are done. We deduce

$$\sup_{s \in \mathbb{C}^+} \|(sI - A)^{-1}\| < \infty.$$

Now the Gaerhard-Prüss-Greiner theorem [21, Thm. V.1.11] says that A generates an exponentially stable semigroup, and this is where we need the fact that H is a Hilbert space. \square

Lemma 2. Let $G = G_- + G_+$, where $G_- \in \mathbf{H}_\infty$ and G_+ has a right coprime factorization $G_+ = NM^{-1}$ over \mathbf{H}_∞ . Then G has also a right coprime factorization over \mathbf{H}_∞ .

Proof. We have $G = G_- + NM^{-1} = (G_-M + N)M^{-1}$, hence with $\tilde{N} = G_-M + N$ we have a factorization $G = \tilde{N}M^{-1}$ over \mathbf{H}_∞ . We show that it is right coprime. Since by assumption $G_+ = NM^{-1}$ is right coprime, there exist $X, Y \in \mathbf{H}_\infty$ such that $XN + YM = I$. Put $\tilde{Y} = Y - XG_-$, then $\tilde{Y} \in \mathbf{H}_\infty$, and $X\tilde{N} + \tilde{Y}M = X(G_-M + N) + (Y - XG_-)M = I$, hence the factorization is right coprime. \square

Remark 1. The authors of [23] propose $h(s) = \left(\frac{s^2+s}{s^2+s+1}\right)^p$ for a pole of order p at 0, and similar expressions apply to poles off the origin. Multiplying with h not only avoids indentations in the Nyquist curve, it also assures that the modified Nyquist curve (4) does not escape to infinity. This is favorable for its approximation by a polygon.

2. Sampled Nyquist test with certificate

In this section we examine how the Nyquist test (4) is implemented. Writing f instead of \tilde{f} , we seek $N \in \mathbb{N}$ and frequencies $\omega_0 = 0 < \omega_1 < \dots < \omega_N = \infty$ such that the closed polygon $P_f = \{f(-j\omega_N), \dots, f(0), f(j\omega_1), \dots, f(j\omega_N)\}$ has the same winding number as the Nyquist curve $\{f(j\omega) : \omega \in \mathbb{R} \cup \{\infty\}\}$. Let $P_f(j\omega)$ denote the linearly interpolated function associated with the polygon, and for any g let $\Delta_{[\omega', \omega'']} \arg g$ denote the change of argument of g along the section $[j\omega', j\omega'']$ of $j\mathbb{R}$. Suppose $f(j\omega) \neq 0$ and $P_f(j\omega) \neq 0$ for all $\omega \in \mathbb{R} \cup \{\infty\}$, then, with the convention $\omega_{-i} = -\omega_i$ we have

$$\text{ind}(f(j\mathbb{R}), 0) = -\frac{1}{2\pi} \sum_{i=-N}^{N-1} \Delta_{[\omega_i, \omega_{i+1}]} \arg f$$

and similarly

$$\begin{aligned} \text{ind}(P_f, 0) &= -\frac{1}{2\pi} \sum_{i=-N}^{N-1} \Delta_{[\omega_i, \omega_{i+1}]} \arg P_f \\ &= -\frac{1}{2\pi} \sum_{i=-N}^{N-1} \arg[f(j\omega_{i+1})/f(j\omega_i)], \end{aligned}$$

the last expression being computable. We now assure that these two winding numbers agree, which is true if the nodes ω_i are chosen such that, for every i ,

$$\Delta_{[\omega_i, \omega_{i+1}]} \arg f = \arg[f(j\omega_{i+1})/f(j\omega_i)]. \quad (8)$$

Geometrically (8) means the closed curve γ_i obtained by concatenating the segment $[f(j\omega_{i+1}), f(j\omega_i)]$ with the piece $f([j\omega_i, j\omega_{i+1}])$ of the Nyquist contour, does not encircle the origin. If $f(s)$ is available analytically, we may, after fixing a small threshold $\delta > 0$, construct the ω_i through the recursion:

$$\omega_{i+1} = \sup \left\{ \omega : \delta + \text{Re} \int_{\omega_i}^{\omega} \frac{f'(j\omega)}{f(j\omega)} d\omega \leq \arg \left[\frac{f(j\omega)}{f(j\omega_i)} \right] \right\}. \quad (9)$$

Alternatively, since $\arg[f(j\omega)/f(j\omega_i)] < \pi$, we may use the following slightly more conservative construction

$$\omega_{i+1} = \sup \left\{ \omega : \delta + \text{Re} \int_{\omega_i}^{\omega} \frac{f'(j\omega)}{f(j\omega)} d\omega \leq \pi \right\}. \quad (10)$$

A third possibility to ensure (8) uses a bound on f' . Call $L[\cdot, \cdot]$ a first-order bound of f if $L[\omega^-, \omega^+] \geq |f'(j\omega)|$ for every $\omega \in [\omega^-, \omega^+]$. Then we have the following simple test.

Lemma 3. Let ω_i, ω_{i+1} denote two consecutive nodes in the polygon P_f not passing through 0, and suppose

$$L[\omega_i, \omega_{i+1}](\omega_{i+1} - \omega_i) < |f(j\omega_i)| + |f(j\omega_{i+1})|. \quad (11)$$

Then condition (8) is satisfied.

Proof. Assume on the contrary that the curve γ_i in (8) encircles the origin. Let ℓ be the length of the curved part $\tilde{\gamma}_i = f([j\omega_i, j\omega_{i+1}])$ of γ_i . The projection line of 0 onto the segment $[f(j\omega_{i+1}), f(j\omega_i)]$ meets the segment at $P_f(j\omega^*)$, $\omega^* \in [\omega_i, \omega_{i+1}]$. But $\tilde{\gamma}_i$ has to cross this line at some point $p \notin [0, P_f(j\omega^*)]$ with $0 \in [p, P_f(j\omega^*)]$, so going from $f(j\omega_i)$ to p , $\tilde{\gamma}_i$ has length $\geq |f(j\omega_i)|$. Similarly, between p and $f(j\omega_{i+1})$ the length of $\tilde{\gamma}_i$ is at least $|f(j\omega_{i+1})|$. Altogether, the length ℓ of $\tilde{\gamma}_i$ exceeds $|f(j\omega_i)| + |f(j\omega_{i+1})|$. But $\ell = \int_{j\omega_i}^{j\omega_{i+1}} |f'(z)| dz = \int_0^1 |f'(j\omega_i + t(j\omega_{i+1} - j\omega_i))| (\omega_{i+1} - \omega_i) dt \leq L[\omega_i, \omega_{i+1}](\omega_{i+1} - \omega_i) < |f(j\omega_i)| + |f(j\omega_{i+1})|$ by hypothesis (11), a contradiction. \square

Remark 2. Consider the case where G, K are stable so that f is holomorphic on a domain containing $\overline{\mathbb{C}^+}$. Assume that f is even holomorphic on $\mathbb{C}_{-\alpha}^+$ for some $\alpha > 0$, which is often the case, e.g. when G is sectorial [20]. By (i) find $\beta > 0$ such that $f(\mathbb{C}_{-\alpha}^+) \subset \mathbb{C}_{-\beta}^+$, and put $\tilde{f}(s) = f(s - \alpha) + \beta$, then $\tilde{f} : \mathbb{C}^+ \rightarrow \mathbb{C}^+$. If $\Gamma = f(\gamma)$, $\gamma = j\mathbb{R}$, is the Nyquist curve, then $\tilde{\Gamma} = \tilde{f}(\tilde{\gamma}) = \Gamma + \beta$, where $\tilde{\gamma} = \alpha + j\mathbb{R}$, and in the place of $\text{ind}(\Gamma, 0)$ we are now interested in $\text{ind}(\tilde{\Gamma}, \beta)$. Put $\sigma(z) = \frac{1+z}{1-z}$ and $\tau(s) = \frac{s-1}{s+1}$, then $\tau = \sigma^{-1}$, and $\phi := \tau \circ \tilde{f} \circ \sigma$ maps the unit disk \mathbb{D} to itself. Now $\gamma_0 = \tau(\tilde{\gamma}) = \left\{ \frac{\alpha-1+j\omega}{\alpha+1+j\omega} : \omega \in \mathbb{R} \right\}$ is the circle with center $\frac{\alpha}{\alpha+1}$ and radius $\frac{1}{\alpha+1}$, the analogue of the Nyquist curve is $\Gamma_0 = \phi(\gamma_0) \subset \mathbb{D}$, and we are interested in $\text{ind}(\Gamma_0, \tau(\beta))$. By the Schwarz-Pick theorem we have $|\phi'(z)| \leq \frac{1-|\phi(z)|^2}{1-|z|^2}$ for $z \in \mathbb{D}$, hence $|\tilde{f}'(s)| \leq \frac{2}{|1+\phi(\tau(s))|^2} \frac{1-|\phi(\tau(s))|^2}{1-|\tau(s)|^2} \frac{2}{|1+s|^2}$. We have to evaluate $f'(j\omega) = \tilde{f}'(\alpha + j\omega)$. Since $f(\alpha + j\omega) = f(j\omega)$ has a limit $\neq 0$ as $\omega \rightarrow \infty$, we have $\phi(\tau(\alpha + j\omega)) \not\rightarrow -1$, so that the term

$$\frac{1-|\phi(\tau(\alpha + j\omega))|^2}{|1+\phi(\tau(\alpha + j\omega))|^2}$$

remains bounded. But $\frac{1}{1-|\tau(\alpha + j\omega)|^2} \frac{1}{|1+\alpha+j\omega|^2} = \frac{1}{4\alpha}$, hence \tilde{f}' is bounded on $\tilde{\gamma} = \alpha + j\mathbb{R}$, and so f' is bounded on $j\mathbb{R}$. Using this, it also follows that ϕ' is bounded on γ_0 . Going back with this information, we find that $|f'(j\omega)| = |\tilde{f}'(\alpha + j\omega)| \leq C\omega^{-2}$ for some computable $C > 0$. This shows that for large ω the next frequency ω^+ for the Nyquist sampling in the test (11) is of the order $\omega^+ \sim \omega + C^{-1}\omega^2|f(j\omega)|$, which explains the extremely fast convergence in algorithm 1. It also follows that the first-order bound $L[\cdot, \cdot]$ is of the form $L[\omega, \omega^+] = C\omega^{-2}$. \blacksquare

Once P_f is constructed, $\text{ind}(P_f, 0)$ is computed by the ray-crossing algorithm: Fix a ray at the origin not passing

through any of the nodes of P_f , and count in a straightforward way the number of signed crossings of that ray by the polygon P_f . The overall Nyquist procedure is presented in algorithm 1.

Algorithm 1. Grid construction and Nyquist stability test

Parameters: $\delta > 0$, $\Theta > 1$.

- ▷ **Step 1** (Initialize). Choose $\omega_0 = 0$ and $\omega_1 > 0$ such that (10), respectively (11), is satisfied.
- ▷ **Step 2** (Extrapolate). Having constructed $\omega_0 < \dots < \omega_i$, put $\omega^\sharp = \Theta(\omega_i - \omega_{i-1}) + \omega_i$. If (10), respectively (11), is satisfied on $[\omega_i, \omega^\sharp]$, then put $\omega_{i+1} = \omega^\sharp$, otherwise use backtracking to find $\omega_{i+1} \in (\omega_i, \omega^\sharp)$ such that (10), respectively (11), holds.
- ▷ **Step 3**. If $\omega_{i+1} < \infty$ loop on with step 2, otherwise obtain Nyquist grid Ω_{nyq} and goto step 4.
- ▷ **Step 4** (Compute winding number). Choose ray starting from 0 which avoids all $f(j\omega_i)$. Then count signed ray crossings of P_f to obtain $\text{ind}(P_f, 0)$.

The following observation gives a justification of our approach.

Theorem 2. Suppose for a given $K \in \mathcal{K}$ the integrals in (10) are computed formally to construct P_f , or a first-order bound $L[\cdot, \cdot]$ for f is used to construct P_f according to rule (11). Then the computation of the winding number is exact, i.e., satisfies $\text{ind}(f, 0) = \text{ind}(P_f, 0)$. In particular, if $\text{ind}(P_f, 0) = -n_p$, then K is certified closed-loop stabilizing. ■

Example 1. Consider study 'DLR1' from the CompLeib collection [19], an open-loop stable rational system $G(s)$ with 10 modes, 2 control inputs and 2 measurements. All modes are badly damped and manifest themselves as sharp peaks in the frequency response with damping not exceeding 5e-3. With $K = [1, -1; -1, 1]$ the system is stable in closed loop, but when moving to $K^+ = [-1 \ 1; 1 \ -1]$, the closed-loop has two unstable modes $0.0041 \pm j0.9951$. Since the number of open-loop poles is $n_p = 0$, we expect the winding number 2 for $f = \det(I + GK^+)$ in (4).

We compute the index via ray-crossing of P_f first on a dense grid $[0, \text{logspace}(-3, 3, 1000)]$, where we get the incorrect value 0. In contrast the grid of algorithm 1 needs only 19 frequencies with (10), and 27 with (11), yet delivers the correct winding number 2, which differs from $n_p = 0$, indicating the arrival of two unstable modes in closed loop. Fig. 1 (left) shows P_f for $f = \det(I + GK^+)$ on the two grids. ■

Remark 3. In Example 1 the closed-loop sensitivity $\|S(K + t(K^+ - K))\|_\infty$ has a bump at $t^* = .78$ on the segment $[K, K^+]$; see Fig. 1 (right). This is where instability occurs. The bump is more or less articulated depending on the frequency grid. This means that $\|S\|_\infty$ serves as a barrier against instability, but not always a reliable one, due to the fact that values descend as t crosses t^* and approaches 1.

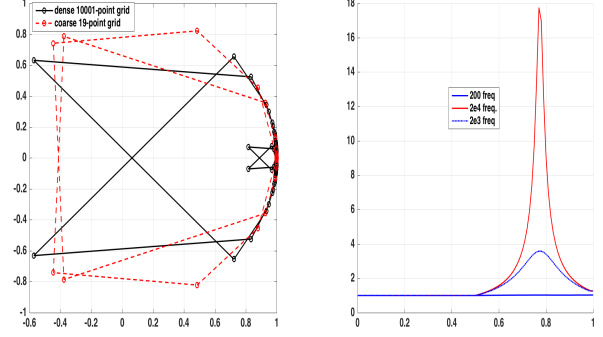


Figure 1. Comparison of logspace and adapted grid Ω_{nyq} for Nyquist (left). Cross section of $\|S\|_\infty$ on segment $[K, K^+]$ (right) for different grids.

3. Optimization method

In this section we present our algorithm for program (2). Let controllers $K \in \mathcal{K}$ be parametrized as $K(\mathbf{x})$ for some vector $\mathbf{x} \in \mathbb{R}^n$ of tunable parameters, and suppose the transfer functions $G(s)$ and $P(s)$ of system and plant are discretized on a sufficiently fine grid $\Omega_{\text{opt}} = \{\omega_0, \dots, \omega_N\}$ for optimization. Then the closed-loop H_∞ -performance to be minimized is $h(\mathbf{x}) = \max_{v=0, \dots, N} \overline{\sigma}(T_{zw}(P_w(j\omega_v), K(j\omega_v, \mathbf{x})))$. As square root of a maximum eigenvalue function, h is locally Lipschitz, but nonsmooth and nonconvex.

Since we do not wish the Nyquist curve $f = \det(I + GK)$ to change its winding number as we update our controller $K(\mathbf{x})$ during optimization, we have to hinder f from crossing 0. Using the sensitivity function $S = (I + GK)^{-1}$, this can be pursued by a constraint $\|S\|_\infty^{-1} \geq r^{-1}$ on the modulus margin, where $r > 0$ is some threshold. In discretized form this is a constraint

$$s(\mathbf{x}) := \max_{v=0, \dots, N} \overline{\sigma} \left[(I + G_w(j\omega_v)K(j\omega_v, \mathbf{x}))^{-1} \right] \leq r. \quad (12)$$

In algorithm 2, instead of calibrating r , we use a dual approach, where we minimize the unconstrained function $g(\mathbf{x}) = \max\{h(\mathbf{x}), as(\mathbf{x})\}$ for some small penalty $a > 0$ over the parameter space $\mathbf{x} \in \mathbb{R}^n$. Since a maximum of H_∞ -norms is again an H_∞ -norm, Clarke subgradients of g may be computed by the method of [1]. We now apply algorithm 2 to minimize g , that is, to solve program (2).

During the following we comment on the salient features of this scheme.

Remark 4. The *primary descent step* \mathbf{x}^+ of step 3 is simply the standard step of the nonsmooth trust-region method [4]. Here \mathbf{x}^+ gives sufficient decrease of g , and would normally be accepted as the next serious iterate. The trouble is that \mathbf{x}^+ may lead to a destabilizing controller $K(\mathbf{x}^+)$.

The difficulty is explained as follows. In the majority of cases the function $s : \mathbf{x} \mapsto \|S(\mathbf{x})\|_\infty$ has a barrier effect as iterates $K(\mathbf{x})$ approach the boundary of stability from inside

Algorithm 2. Non-smooth optimization for (2)

- ▷ **Step 1** (Initialize). Find initial stabilizing controller $K(\mathbf{x}^0)$, put counter $j = 0$, and determine number n_p of open-loop rhp poles for Nyquist test. Initialize trust-region radius as $R_1 > 0$.
- ▷ **Step 2** (Local model). Given current iterate \mathbf{x}^j at counter j , compute a local polyhedral model $\phi(\cdot, \mathbf{x}^j)$ of g at \mathbf{x}^j .
- ▷ **Step 3** (Primary descent). Starting with trust-region radius R_j and model ϕ , use trust-region update mechanism in tandem with local model update to generate a primary descent step \mathbf{x}^+ for g . Procedure ends with new trust-region radius R^+ , and new local model $\phi^+(\cdot, \mathbf{x}^j)$.
- ▷ **Step 4** (Nyquist test). Use Nyquist test in algorithm 1 to check whether $K(\mathbf{x}^+)$ is closed-loop stabilizing. If this is the case (i.e., $\text{ind}(P_f, 0) = -n_p$), then put $\mathbf{x}^{j+1} = \mathbf{x}^+$ and $R_{j+1} = R^+$, increase counter j , and loop on with step 2. In case of instability ($\text{ind}(P_f, 0) \neq -n_p$), goto step 5.
- ▷ **Step 5** (Stability safeguard). Reject descent step \mathbf{x}^+ , reduce trust-region radius to $R^{++} = R^+/2$, and add a repelling cutting plane to the local model ϕ^+ to obtain ϕ^{++} . Then go back to step 3 with initial information R^{++} , ϕ^{++} instead of R_j and ϕ .

(see Fig. 1 right). But in contrast with classical barrier functions like the log-barrier in interior point methods, $s(\mathbf{x})$ takes on finite values behind the barrier and outside the domain of stability. This means it cannot be fully relied on to enforce stability, as seen in Example 1. This is why it is used in tandem with the Nyquist test.

Remark 5. In the original approach [1, 24] to nonsmooth H_∞ -synthesis the closed-loop system matrix $A(K)$ is available, so that closed-loop stability can be implemented using the spectral abscissa: a constraint $\alpha(A(K(\mathbf{x}))) \leq -\varepsilon$ is added, which not only serves to *recognize* instability, but also allows to *repel* steps from becoming unstable. In contrast, our Nyquist test allows to detect instability, but since the winding number is a discrete quantity, it cannot be used as a constraint to generate the repelling effect. The latter is implemented through the barrier property of the sensitivity function (12). Backtracking from the unstable \mathbf{x}^+ toward the stable \mathbf{x}^j , we locate an intermediate stable value $\mathbf{x}_t = t\mathbf{x}^j + (1-t)\mathbf{x}^+$, for which $s(\mathbf{x}_t)$ is large but $K(\mathbf{x}_t)$ is still stabilizing. Then we generate a cutting plane of $s(\cdot)$ at \mathbf{x}_t , which we add to the model ϕ^+ . Ideally, this plane is relatively steep and therefore builds the desired barrier effect into the improved model ϕ^{++} .

Remark 6. Step 1 requires that G can be stabilized by a structured controller $K_0 \in \mathcal{K}$. This is a stronger hypothesis than in (iv). Even for finite-dimensional systems it is generally difficult to *decide* whether a stabilizing controller of a given

structure \mathcal{K} exists. The problem is known to be NP-hard for static, reduced fixed-order, or PID controllers. However, this is a worst-case result which is somewhat in contrast with the fact that practical systems are usually easy to stabilize even with structured laws.

Note that when G is already stable, an initial stabilizing controller is obtained by the small gain condition $\|K(s)\|_\infty < 1/\|G(s)\|_\infty$. This guarantees $\mathcal{T} \in \mathbf{H}_\infty$ in (6), and then internal stability under the hypotheses of Theorem 1.

Remark 7. Convergence analysis of the trust-region algorithm is outside the scope of this work and can be based on [4]. Note that due to nonsmoothness special care has to be taken, as the standard trust-region scheme based on the Cauchy point fails. The success of the method hinges on building a good polyhedral model of the objective at the current iterate based on cutting planes. We refer to [1], where this is discussed.

4. Sampling for synthesis with certificate

As we have seen, Nyquist stability (4) can be based on the relatively coarse grid Ω_{nyq} of algorithm 1. This typically requires significantly less than 100 nodes for most plants, but Ω_{nyq} must at each step be re-adapted to the candidate controller $K(\mathbf{x})$, because the tunable parameters \mathbf{x} move during optimization. In contrast, the grid for optimization Ω_{opt} used in algorithm 2 has to be of finer scale, but it remains invariant during optimization, as updating it would change problem (2).

An initial stabilizing controller $K(\mathbf{x}_0)$ can be used to build an initial grid Ω_{opt} , but we have to be aware that the controller $K(\mathbf{x})$, which varies in the course of optimization, may by itself develop resonant modes, which may render the original sampling $\omega_i \in \Omega_{\text{opt}}$ inappropriate. In order to prevent this phenomenon, it is cautious to optimize over classes \mathcal{K} of *stable* controllers, and to put *constraints on the damping* of the controller modes, confining them to a conical region in \mathbb{C}^- . For real-rational controllers with explicit state-space realization (3) such constraints are readily implemented and added in (2). Stability of K translates into $\alpha(A_K(\mathbf{x})) \leq -\varepsilon$ for some threshold $\varepsilon > 0$, and similarly, the mode damping requirement becomes a constraint $\alpha_{\triangleright}(A_K(\mathbf{x})) \leq -r$ as soon as we define a conical analogue of the spectral abscissa via

$$\alpha_{\triangleright}(A) = \max\{\text{Re}(\lambda)/|\lambda| : \lambda \text{ eigenvalue of } A\},$$

and where r accounts for the aperture of the conical section. Subgradients of α and α_{\triangleright} are computed as in [25, 26].

Even with these precautions, upgrading Ω_{opt} may become necessary, and we now discuss a method to adapt a grid Ω_{opt} to a candidate controller $K \in \mathcal{K}$.

Lemma 4. Let $\phi : \mathbb{R} \rightarrow \mathbb{R}_+$ be of class C^1 , and let $L[\cdot, \cdot]$ be a first-order bound for ϕ . Let ω_i, ω_{i+1} be two consecutive nodes of a piecewise linear interpolation P_ϕ of ϕ such that

$\gamma^* \geq \max\{\phi(\omega_i), \phi(\omega_{i+1})\}$ and for a given tolerance $\vartheta > 0$,

$$L[\omega_i, \omega_{i+1}](\omega_{i+1} - \omega_i) < 2\gamma^* + 2\vartheta - \phi(\omega_i) - \phi(\omega_{i+1}). \quad (13)$$

Then $\phi(\omega) < \gamma^* + \vartheta$ for every $\omega \in [\omega_i, \omega_{i+1}]$.

Proof. Suppose on the contrary that there exists $\omega^* \in [\omega_i, \omega_{i+1}]$ such that $\phi(\omega^*) \geq \gamma^* + \vartheta$. Then the polygon connecting $\phi(\omega_i), \phi(\omega^*), \phi(\omega_{i+1})$ has length $\geq L$, $L = \sqrt{A^2 + (\omega^* - \omega_i)^2} + \sqrt{B^2 + (\omega_{i+1} - \omega^*)^2}$, where $A = \gamma^* + \vartheta - \phi(\omega_i)$ and $B = \gamma^* + \vartheta - \phi(\omega_{i+1})$. We have $L \geq \ell = \sqrt{(A+B)^2 + (\omega_{i+1} - \omega_i)^2}$, the minimum being attained at $\omega^* = \frac{\omega_i B + \omega_{i+1} A}{A+B}$. But the curve $\{(\omega, \phi(\omega)) : \omega \in [\omega_i, \omega_{i+1}]\}$ has length

$$\mathcal{L} = \int_{\omega_i}^{\omega_{i+1}} \sqrt{1 + \phi'(\omega)^2} d\omega \leq \sqrt{1 + L[\omega_i, \omega_{i+1}]^2} (\omega_{i+1} - \omega_i),$$

and $\mathcal{L} \geq L \geq \ell$, so we get the estimate $\sqrt{1 + L[\omega_i, \omega_{i+1}]^2} \geq \sqrt{(A+B)^2 / (\omega_{i+1} - \omega_i)^2 + 1}$, which contradicts (13). \square

Algorithm 3. Infinite-dimensional H_∞ -synthesis

Parameters: Tolerance $\vartheta > 0$.

- ▷ **Step 1** (Grid for optimization). Use initially stabilizing controller $K_0 \in \mathcal{K}$ and first-order bound condition (13) for function $\phi(\omega) = \overline{\sigma}(T_{wz}(P(j\omega), K_0(j\omega)))$ to construct grid Ω_{opt} .
- ▷ **Step 2** (Optimize). Using algorithm 2, compute optimal controller $K^* \in \mathcal{K}$ on grid Ω_{opt} with value γ^* .
- ▷ **Step 3** (Refined grid). Use first-order bound $L[\cdot, \cdot]$ for $\phi(\omega) = \overline{\sigma}(T_{wz}(P(j\omega), K^*(j\omega)))$ to check whether grid Ω_{opt} satisfies (13). If not add nodes to assure this and obtain verification grid Ω_{ver} with this property.
- ▷ **Step 4** (Verify). Check $\gamma^* \geq \max_{\Omega_{\text{ver}}} \overline{\sigma}(T_{wz}(P, K^*)) - \vartheta$. If this is the case quit successfully, otherwise replace Ω_{opt} by $\Omega_{\text{opt}} \cup \Omega_{\text{ver}}$ and go back to step 2.

As we shall see in the sequel, $\vartheta > 0$ serves as the tolerance within which we are able to know the value of the infinite-dimensional (un-sampled) H_∞ -norm $\|T_{wz}(P, K)\|_\infty$. In order to derive this, we have to apply the test (13) to the performance function $\phi(\omega) = \overline{\sigma}(T_{wz}(P(j\omega), K(j\omega)))$, and for that we have to analyze its differentiability. Consider the one-parameter family of symmetric matrices

$$\omega \mapsto \mathcal{M}(\omega) = T_{wz}(P(j\omega), K(j\omega))^H T_{wz}(P(j\omega), K(j\omega)),$$

then by [27, Theorem 6.1] the eigenvalues $\lambda_v(\omega)$ of $\mathcal{M}(\omega)$ are real analytic functions, hence ϕ^2 is a finite maximum of real analytic eigenvalue functions, and since $\phi > 0$, we deduce that ϕ as well is a finite maximum of real-analytic functions. What is even more important is the following:

Lemma 5. [3, Theorem 2.3] ϕ has only finitely many points of non-smoothness, and is of class C^2 at peak frequencies. \square

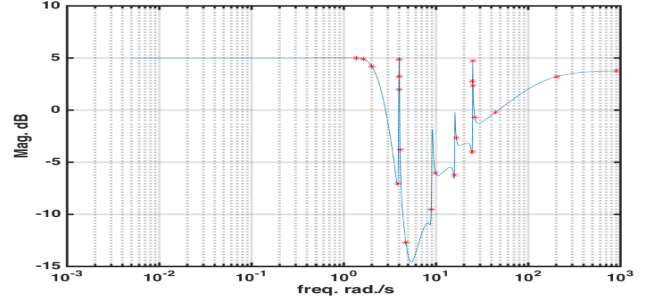


Figure 2. Verification grid Ω_{ver} via (13), with $\gamma^* = 1.78$ and $\vartheta = 10^{-2}$. As expected flat parts need few grid points ω_i , whereas resonances are perfectly captured.

In consequence, there exists $\vartheta_0 > 0$ such that ϕ is of class C^2 on $\{\omega : \phi(\omega) > \|T_{wz}(P, K)\|_\infty - \vartheta_0\}$. This leads to

Theorem 3. If $0 < \vartheta \leq \vartheta_0$ and a first-order bound $L[\cdot, \cdot]$ for $\phi = \overline{\sigma}(T_{wz}(P, K^*))$ in tandem with rule (13) is used in step 4 of algorithm 3, then the gain γ^* achieved by K^* is certified to satisfy

$$\gamma^* \geq \|T_{wz}(P, K^*)\|_\infty - \vartheta.$$

■

Remark 8. In practice it is usually sufficient to generate a numerical upper bound $L[\cdot, \cdot]$ using a finite-difference approximation $\phi'(\omega) \approx (\phi(\omega^+) - \phi(\omega^-)) / (\omega^+ - \omega^-)$. In our testing this gives excellent results and leads to moderately sized grids Ω_{opt} and Ω_{ver} . Fig. 2 gives a typical case.

Remark 9. To generate the optimization grid Ω_{opt} we apply (13) with $\gamma^* = \max\{\phi(\omega_i), \phi(\omega_{i+1})\}$ on each interval $[\omega_i, \omega_{i+1}]$. When it comes to just certifying the optimal value $h(\mathbf{x}^*) = \|T_{wz}(K(\mathbf{x}^*))\|_{\infty, d} = \phi(\omega^*)$ in step 4 of algorithm 3, we can construct an even coarser grid by applying (13) with $\gamma^* = \phi(\omega^*)$ on every $[\omega_i, \omega_{i+1}]$. Here our grid turns out sparse at frequencies $\phi(\omega) \ll \phi(\omega^*)$, while resonances are still accurately captured (see Fig. 2 for an illustration). We call this a verification grid Ω_{ver} . The outlined method to construct Ω_{opt} , and to complete it in step 6 by adding elements of a verification grid Ω_{ver} , is well-suited to discretize the controller design problem (1). Discretization at that level avoids the pitfalls in system reduction and identification techniques.

We can further exploit Lemma 4 to obtain information on how close the values γ^* of (2), and γ_∞ of (1), are. Writing $h(\mathbf{x}) = \|T_{wz}(K(\mathbf{x}))\|_{\infty, d}$ for the discrete H_∞ -norm of (2) on Ω_{opt} , and $h_\infty(\mathbf{x}) = \|T_{wz}(K(\mathbf{x}))\|_\infty$ for the true H_∞ -norm in (1), we have the following:

Corollary 1. Let \mathbf{x}_∞ be a local minimum of the infinite-dimensional H_∞ -program with value γ_∞ , and \mathbf{x}^* a local minimum of (2) with value γ^* . Suppose a first-order bound in tandem with rule (13) is used in step 6 of algorithm 3. Then

if \mathbf{x}^* , \mathbf{x}_∞ are within neighborhoods of local optimality of each other, we have $h(\mathbf{x}_\infty) \geq h(\mathbf{x}^*) \geq h_\infty(\mathbf{x}^*) - \vartheta \geq h_\infty(\mathbf{x}_\infty) - \vartheta \geq h(\mathbf{x}_\infty) - \vartheta$.

Proof. Indeed, $h(\mathbf{x}_\infty) \geq h(\mathbf{x}^*)$ because \mathbf{x}^* is a minimum of h on a neighborhood $U(\mathbf{x}^*)$, and $\mathbf{x}_\infty \in U(\mathbf{x}^*)$ by hypothesis. Next $h(\mathbf{x}^*) \geq h_\infty(\mathbf{x}^*) - \vartheta$ by Lemma 4, because construction of the grid uses the bound $L[\cdot, \cdot]$ and rule (13). Next $h_\infty(\mathbf{x}^*) \geq h_\infty(\mathbf{x}_\infty)$, because \mathbf{x}_∞ is a minimum of h_∞ on a neighborhood $U(\mathbf{x}_\infty)$, and $\mathbf{x}^* \in U(\mathbf{x}_\infty)$ by hypothesis. The last inequality is satisfied because $h \leq h_\infty$. \square

This means comparable locally optimal values of the infinite dimensional H_∞ -program (1) and its approximation (2) differ by at most ϑ , our a priori chosen tolerance. Since most of the time our algorithm finds even the global minimum of (2), this is a very useful information in practice, as the value γ_∞ of a global solution of the infinite dimensional H_∞ -program is then known within the prior tolerance ϑ .

The result of Theorem 3 could also be explained as follows. Suppose \mathbf{x}^* is a local minimum of (2), i.e., $h(\mathbf{x}) \geq h(\mathbf{x}^*)$ for every \mathbf{x} in some neighborhood U of \mathbf{x}^* . We know that $h \leq h_\infty$, so the value $\gamma^* = h(\mathbf{x}^*)$ is *a priori* optimistic. Could it be overly optimistic (i.e. could it be way too low) and therefore misleading? The answer is no.

Corollary 2. Let γ_∞ be the best value of program (1) on U , that is $\gamma_\infty = \inf\{h_\infty(\mathbf{x}) : \mathbf{x} \in U \text{ admissible in (1)}\}$. Then $\gamma^* \leq \gamma_\infty \leq \gamma^* + \vartheta$.

Proof. Since $h \leq h_\infty$ we have $\gamma^* = \inf_U h \leq \inf_U h_\infty = \gamma_\infty$. Fix $\varepsilon > 0$, then there exists $\mathbf{x}_\infty \in U$ such that $\gamma_\infty \geq h_\infty(\mathbf{x}_\infty) - \varepsilon$. By Theorem 3 we have $\gamma^* \geq h_\infty(\mathbf{x}^*) - \vartheta \geq \gamma_\infty - \vartheta \geq h_\infty(\mathbf{x}_\infty) - \vartheta - \varepsilon \geq h(\mathbf{x}_\infty) - \vartheta - \varepsilon \geq h(\mathbf{x}^*) - \vartheta - \varepsilon = \gamma^* - \vartheta - \varepsilon$, and since ε is arbitrary, this implies $\gamma^* \geq \gamma_\infty - \vartheta \geq \gamma^* - \vartheta$. \square

5. Illustrating remarks and examples

From a practical point of view, having to check (iv) prior to computations is annoying. In finite dimensions the optimization method leads directly to an exponentially stabilizing H_∞ -controller $K^* \in \mathcal{K}$. What restrains us here from proceeding in the same way is that exponential stabilizability and detectability are used in the proof of Theorem 1 to pass from external stability to internal stability. Here external stability means $\mathcal{T} \in \mathbf{H}_\infty$ for the \mathcal{T} in (6). The following result could therefore be considered a practical workaround.

Theorem 4. Suppose $G(s), K(s)$ satisfy assumptions (i) - (iii), (v). Let $G(s) - G(\infty) = \mathcal{O}(s^{-r})$ for some $r > \frac{1}{2}$ as $s \rightarrow \infty$ on $\overline{\mathbb{C}}^+$, and suppose $K^* \in \mathcal{K}$ is computed by algorithm 3, hence satisfies (4). Then the closed loop is externally stable. Moreover, $G(s)$ admits a state-space realization with regard to which the closed loop with K^* is exponentially stable.

Proof. By [28], the strictly proper $G - G(\infty)$ has coprime factorizations over $\overline{\mathbb{C}}^+$, and hence so has $G(s)$. We can therefore

go directly to part 2) of the proof of Theorem 1. By assumption optimization terminates successfully with $K^* \in \mathcal{K}$ satisfying (4). Then as in part 2) of the proof of Theorem 1 we deduce $\mathcal{T} \in \mathbf{H}_\infty$, i.e., the closed loop is externally stable. In addition, by [29, Thm. 4.4 (ii)] \mathcal{T} has a jointly exponentially stabilizable and detectable state-space realization. By Theorem 1 this realization in closed loop with that of K^* is exponentially stable. \square

Remark 10. Consider a parabolic PDE with Dirichlet boundary control

$$z_t + \sum_{|\alpha|, |\beta| \leq m} (-1)^{|\alpha|} D^\alpha (a_{\alpha\beta} D^\beta z) = 0 \text{ on } Q \times \mathbb{R}_+,$$

$$D_\nu^i z(\xi, t) = \sum_{k=1}^N \varphi_{ik}(\xi) u_{ik}(t), \quad \xi \in \partial Q, i = 0, \dots, m-1$$

with uniform ellipticity condition, $a_{\alpha\beta} \in C^\infty$, and ∂Q a compact orientable C^∞ -manifold. By [30] the problem may be rewritten in state-space form $\dot{x} = Ax + Bu$, where A generates an analytic semigroup, $u = (u_{ik})$ and

$$Bu(\xi, t) = \sum_{i=0}^{m-1} \sum_{k=1}^N B_i \phi_\xi(\cdot) u_{ik}(t)$$

with bounded operators B_i . If the output operator is also chosen of finite rank, like for instance $y = (y_1, \dots, y_m)$ with $y_\ell(t) = \int_Q c_\ell(\xi) z(\xi, t) d\xi$, then all hypotheses (i) - (iii) are satisfied, and what remains to be done in a specific situation is choosing a class \mathcal{K} with property (v), and assuring exponential stabilizability and detectability by the choice of the basis functions. Computation of $G(s)$ for fixed s is then reduced to solving elliptic Dirichlet boundary value problems

$$\sum_{1 \leq |\alpha|, |\beta| \leq m} (-1)^{|\alpha|} D^\alpha (a_{\alpha\beta} D^\beta z) + (a_{00} + s)z = 0 \text{ on } Q$$

(14)

$$D_\nu^i z(\xi, s) = \phi_{ik}(\xi), \quad \xi \in \partial Q$$

and letting $G_{ik\ell}(s) = y_\ell(s)/u_{ki}(s) = \int_Q c_\ell(\xi) z(\xi, s) d\xi$. Note that $G'(s)$, required in (13), can also be computed by a similar elliptic boundary value problem obtained by differentiating (14) with respect to s .

The only restriction in this approach is that boundary control and output are of finite rank, as otherwise the controller would not be implementable.

Example 2. We consider boundary control of heat flow in a one-dimensional medium

$$x_t(\xi, t) - x_{\xi\xi}(\xi, t) = 0, \quad 0 \leq \xi \leq 1, t \geq 0$$

with initial conditions $x(\xi, 0) = 0$ and boundary control

$$x_\xi(0, t) = 0, \quad x_\xi(1, t) = u(t),$$

where $u(t)$ is the rate of heat flow into the medium at the end $\xi = 1$. As measurement we take $y(t) = x(\xi_0, t)$ at some position $0 \leq \xi_0 \leq 1$. Following [20, Example 4.3.12], the transfer function $G(s) = y(s)/u(s)$ is

$$G(s) = \frac{1}{s} + 2 \sum_{v=1}^{\infty} \frac{(-1)^v \cos(v\pi\xi_0)}{s + v^2\pi^2}$$

from which we see that G is strictly proper and meromorphic, but not stable due to the pole at 0. Before we apply the Nyquist test, we check hypothesis (v). To see that (A, B) is stabilizable we take the state feedback law $u(t) = -\alpha x(1, t)$ with $\alpha = \sqrt{k} \tan \sqrt{k} > 0$ for some $k \in (0, \frac{\pi}{2})$, then the state evolves as $x(\xi, t) = x(0, 0)e^{-kt} \cos \sqrt{k}\xi$, which decays exponentially in t uniformly over $\xi \in [0, 1]$.

For detectability, we have to find a law $F : h(t) \mapsto v(\xi)h(t)$ such that $x_t = x_{\xi\xi} + v(\xi)x(\xi, t)$ with boundary conditions $x_\xi(0, t) = 0 = x_\xi(1, t)$ is stable, and that works similarly. Experiments with this example are included in Section 9. For the setup of boundary control problems see also [30, 31]. ■

Remark 11. Not unexpectedly, hyperbolic boundary control problems are more mulish with regard to applicability of our method, as is explained by the well-known fact [32] that for two and more space dimensions the infinitesimal generator need no longer satisfy the spectrum determined growth condition. For hyperbolic equations of spatial dimension one [33] proves validity of the spectral mapping theorem, so that spectrum determined growth is assured in open loop. However, since spectrum determined growth is not even invariant under compact perturbations, we have no easy means to know whether the closed loop still has this property.

Remark 12. In Theorems 1 and 4 we achieve exponential stability in closed loop, which is important when $G(s)$ is the transfer function of the linearization about steady-state of a non-linear infinite-dimensional process, because then we derive a certificate of local exponential stability of that non-linear system in closed loop; cf. [34]. This is no longer true for weaker spectrum-determined notions of stability in linear system theory, like strong stability [21].

6. Application in process control

We apply our frequency-sampled H_∞ -synthesis method to control a continuous cooling crystallizer, shown schematically in Fig. 3. The process uses fines dissolution and product removal, and is governed by a population balance and a molar balance equation; see [35, 36]. The population balance is of the form

$$\frac{\partial n(L, t)}{\partial t} = -G(c(t)) \frac{\partial n(L, t)}{\partial L} - \frac{q}{V} h_{fp}(L) n(L, t) \quad (15)$$

$$n(L, 0) = n_0(L), \quad n(0, t) = \frac{B(c(t))}{G(c(t))} \quad (16)$$

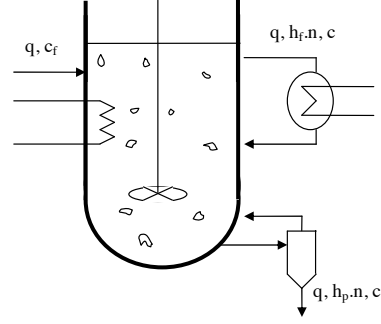


Figure 3. Continuous KCl-crystallizer with solute feed c_f , fines dissolution h_f , and product removal h_p . Solute concentration $c(t)$ is stabilized at steady-state by control of solute feed $c_f(t)$.

where $n(L, t)$ is the crystal size distribution (CSD), $c(t)$ is the solute concentration, and the classification functions specifying fines dissolution and product removal are $h_f(L) = R(1 - h(L - L_f))$, $h_p(L) = 1 + zh(L - L_p)$, $h_{fp} = h_f + h_p$, where h is the unit-step function. The crystal growth and birth coefficients obey phenomenological laws

$$G(c) = k_g (c - c_s)^g, \quad B(c) = k_b (c - c_s)^b.$$

The molar balance is an integral-differential equation of the form

$$M \frac{dc}{dt} = \frac{q(\rho - Mc)}{V} + \frac{\rho - Mc}{\varepsilon} \frac{d\varepsilon}{dt} + \frac{qMc_f}{V\varepsilon} - \frac{q\rho}{V\varepsilon} - \frac{q\rho z\eta}{V\varepsilon}, \quad (17)$$

with initial condition $c(0) = c_0$, where

$$\varepsilon(t) = 1 - k_v \int_0^\infty n(L, t) L^3 dL, \quad \eta(t) = k_v \int_{L_p}^\infty n(L, t) L^3 dL.$$

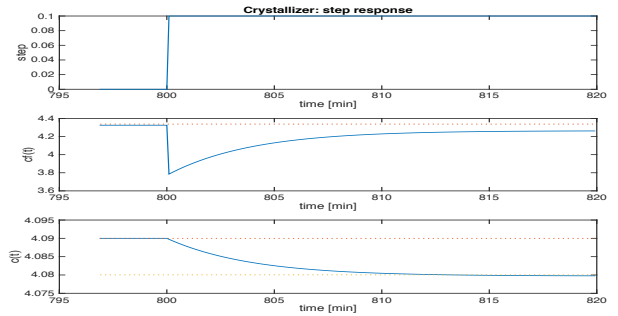


Figure 4. Open loop step response of nonlinear model

The steady state equations lead to the explicit relationship

$$Mc_{fss} = \rho(1 + z\eta_{ss}) - (\rho - Mc_{ss})\varepsilon_{ss}$$

where

$$\varepsilon_{ss} = 1 - k_v \int_0^\infty n_{ss}(L) L^3 dL, \quad \eta_{ss} = k_v \int_{L_p}^\infty n_{ss}(L) L^3 dL$$

Crystallizer data

feed rate	q	0.05	ℓ/min
total volume	V	10.5	ℓ
fines removal size	L_f	0.2	mm
product removal size	L_p	1.0	mm
fines removal rate	R	5.0	---
product removal rate	z	2.0	---
growth rate constant	k_g	0.0305	$\text{mm}\ell/\text{min} \cdot \text{mol}$
growth rate exponent	g	1	---
nucleation rate	k_b	8.36e9	$\ell^3/\text{min} \cdot \text{mol}^4$
nucleation rate exponent	b	4	---
crystal density	ρ	1989	g/ℓ
molar mass	M	74.551	g/mol
volumetric shape factor	k_v	1.112e-7	ℓ/mm^3
saturation concentration	c_s	4.038	mol/ℓ
crystal size distribution	$n(L, t)$		$\#/\text{mm} \cdot \ell$
solute concentr. in liquid	$c(t)$		mol/ℓ
solute feed concentration	$c_f(t)$		mol/ℓ

Table 1. Crystallizer parameters

with

$$n_{ss}(L) = \frac{B(c_{ss})}{G(c_{ss})} e^{-\frac{q}{V G(c_{ss})} H_{fp}(L)}, H_{fp}(L) = \int_0^L h_{fp}(\ell) d\ell,$$

and where our experiment uses $c_{ss} = 4.09$. Parameters are gathered in Table 1. The control input is solute feed concentration $c_f(t)$, the measured output is molar concentration $c(t)$.

Linearization about steady state with $n(L, t) = n_{ss}(L) + \Delta n(L, t)$, $c(t) = c_{ss} + \Delta c(t)$, $c_f(t) = c_{fss} + \Delta c_f(t)$, $\varepsilon(t) = \varepsilon_{ss} + \Delta \varepsilon(t)$, $\eta(t) = \eta_{ss} + \Delta \eta(t)$ leads to the linearized population balance

$$\Delta n_t = -k_g n'_{ss}(L) \Delta c - G(c_{ss}) \Delta n_L - \frac{q}{V} h_{fp}(L) \Delta n \quad (18)$$

with initial condition $\Delta n(L, 0) = 0$ and boundary condition

$$\Delta n(0, t) = \frac{3k_b}{k_g} (c_{ss} - c_s)^2 \Delta c(t), \quad (19)$$

and the linearized molar balance

$$\begin{aligned} \Delta c' = & -\frac{q}{V} \Delta c + \frac{q}{V \varepsilon_{ss}} \Delta c_f + \frac{\rho - M c_{ss}}{M \varepsilon_{ss}} \Delta \varepsilon' \\ & + \frac{q\rho - qM c_{fss} + q\rho z \eta_{ss}}{V M \varepsilon_{ss}^2} \Delta \varepsilon - \frac{q\rho z}{V M \varepsilon_{ss}} \Delta \eta \end{aligned} \quad (20)$$

with $\Delta c(0) = 0$,

$$\begin{aligned} \Delta \varepsilon(t) = & -k_v \int_0^\infty \Delta n(L, t) L^3 dL, \\ \Delta \eta(t) = & k_v \int_{L_p}^\infty \Delta n(L, t) L^3 dL. \end{aligned}$$

The infinite dimensional transfer function $G_{\text{cry}}(s) := \Delta c(s)/\Delta c_f(s)$ is now computed formally as

$$G_{\text{cry}}(s) = \frac{p_{12}(s)}{p_{13}(s) + q_{12}(s) e^{-\frac{sL_f}{G(c_{ss})}} + r_{12}(s) e^{-\frac{sL_p}{G(c_{ss})}}}, \quad (21)$$

where $p_{12}, q_{12}, r_{12}, p_{13}$ are polynomials of order 12 respectively 13. In particular, G_{cry} is meromorphic and strictly proper. If a class \mathcal{H} of real rational proper controllers is used, hypotheses (i)–(iii), (v) are satisfied.

Before we apply our method, we verify hypothesis (iv). We write the linearized system in the form

$$\begin{bmatrix} \Delta n_t \\ \Delta c' \end{bmatrix} = \begin{bmatrix} \mathcal{D} & \mathcal{M} \\ \mathcal{I} & \delta \end{bmatrix} \begin{bmatrix} \Delta n \\ \Delta c \end{bmatrix} + \begin{bmatrix} 0 \\ \gamma \end{bmatrix} \Delta c_f \quad (22)$$

where $\delta = -q/V - k_g \int_0^\infty n'_{ss}(L) L^3 dL$, and $\gamma = q/V \varepsilon_{ss}$ are constants, and $\mathcal{D} = -G(c_{ss}) \frac{\partial}{\partial L} - (q/V) h_{fp}(L)$ is an unbounded differential operator on the Hilbert space

$$\mathcal{H} = L^2((0, \infty), \max\{1, L^3\} dL),$$

while $\mathcal{M} : \mathbb{R} \rightarrow \mathcal{H}$, $\Delta c \mapsto -k_g n'_{ss}(L) \Delta c$ is a multiplication operator, and $\mathcal{I} : \mathcal{H} \rightarrow \mathbb{R}$ is the bounded linear integral operator we obtain when we substitute the population balance equation to obtain $\Delta \varepsilon'(t) = -k_g \Delta c(t) \int_0^\infty n'_{ss}(L) L^3 dL + \int_0^\infty \frac{q}{V} h_{fp}(L) L^3 \Delta n(L, t) dL + G(c_{ss}) \int_0^\infty \Delta n_L(L, t) L^3 dL$. For the last term we use partial integration to obtain

$$-3G(c_{ss}) \int_0^\infty \Delta n(L, t) L^2 dL,$$

so that altogether $\mathcal{I}[\Delta n] = \int_0^\infty \Delta n(L, t) \phi(L) dL$ for an expression $\phi(L)$ gathering weighted terms containing $L^2, L^3, h_{fp}(L) L^3$, and $\chi_{[L_p, \infty)}(L) L^3$ in (20). Setting $A = [\mathcal{D}, \mathcal{M}; \mathcal{I}, \delta]$, we have $D(A) = \{(u, v) \in \mathcal{H} \times \mathbb{R} : \frac{\partial u}{\partial L} \in \mathcal{H}, u(0) = (3k_b/k_g)(c_{ss} - c_s)^2 v\}$, we see that A generates a strongly continuous semigroup of operators on a Hilbert space, while the input operator $B = [0; \gamma]$ is of finite rank. The same is true for the output operator $C = [0, 1]$. It remains to check that (A, B, C) is exponentially stabilizable and detectable.

Lemma 6. *The system (18), (20) with boundary condition (19) is exponentially stabilizable and detectable.*

Proof. For stabilizability the idea is to set up a linear integral operator \mathcal{K} in state-feedback form $\frac{q}{V \varepsilon_{ss}} \Delta c_f(t) = \mathcal{K}[\Delta n, \Delta c](t)$ such that

$$\begin{aligned} \mathcal{K}[\Delta n, \Delta c] = & -\frac{\rho - M c_{ss}}{M \varepsilon_{ss}} \Delta \varepsilon' \\ & - \frac{q\rho - qM c_{fss} + q\rho z \eta_{ss}}{V M \varepsilon_{ss}^2} \Delta \varepsilon + \frac{q\rho z}{V M \varepsilon_{ss}} \Delta \eta. \end{aligned}$$

Because then substituting this control law in (20) leads to the equation $\Delta c' = -\frac{q}{V} \Delta c$, which is exponentially stable. Substituting Δc back in (18) is then stable, because the differential operator $\mathcal{D} = -G(c_{ss}) \frac{\partial}{\partial L} - \frac{q}{V} h_{fp}(L)$ with boundary condition (19) is exponentially stable. Checking boundedness of \mathcal{K} is analogous to checking boundedness of the integral operator \mathcal{I} above.

Concerning exponential detectability, in matrix notation the system may be written as

$$\begin{bmatrix} \Delta n_t \\ \Delta c' \end{bmatrix} = \left(\begin{bmatrix} \mathcal{D} & \mathcal{M} \\ \mathcal{I} & \delta \end{bmatrix} + \begin{bmatrix} \mathcal{G} \\ \eta \end{bmatrix} [0 \ 1] \right) \begin{bmatrix} \Delta n \\ \Delta c \end{bmatrix}$$

where $\mathcal{I}, \mathcal{D}, \mathcal{M}, \delta$ are as in (22), $C = [0 \ 1]$, and $\mathcal{F} = [\mathcal{G}; \eta]$ is sought. We choose $\mathcal{G} = -\mathcal{M}$, then the first equation becomes the exponentially stable $\Delta n_t = -G(c_{ss})\Delta n_L - \frac{q}{h}h_{fp}(L)\Delta n_L$, with boundary condition (19), which was already encountered in the previous proof. Substituting this back, the second equation becomes $\Delta c' = (\delta + \eta)\Delta c + r(t)$, which can be stabilized by choosing $\delta + \eta < 0$. That gives the required $\mathcal{F} = [\mathcal{G}; \eta]$. \square

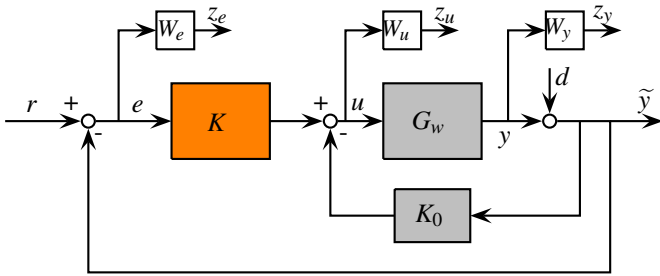


Figure 5. Control configuration for continuous crystallizer.

A first application of algorithm 1 reveals two unstable poles of G_{cry} . Using `systune` based on [1] we compute a static controller K_0 which stabilizes a low-order finite-difference crystallizer model G_{502} with 502 states, where the target decay rate is chosen as $1e-7$. Using algorithm 1, we then confirm that K_0 also stabilizes the infinite dimensional $G_{\text{cry}}(s)$.

In order to optimize performance of the continuous crystallizer, G_{cry} is sampled as in algorithm 3, and the method is applied to $G = \mathcal{F}_1(G_{\text{cry}}, K_0)$, which has $n_p = 0$ rhp poles. We use the scheme of Fig. 5 with K_0 held fixed, while $K \in \mathcal{K}$ is optimized over the class $\mathcal{K}_{2,\text{stab}}$ of stable second-order controllers. The H_∞ -channel is $(r, d) \rightarrow (z_e, z_u, z_y)$ with weighing filters $W_e(s) = \frac{0.1s+0.199}{s+0.00199}$, $W_u = 0.01$, $W_y = \frac{100000s+1.333e04}{s+4.216e-06}$, and the optimal H_∞ -controller achieves a gain of $\gamma_\infty = 1.18$. The optimal controller of order 2 so obtained is

$$K^*(s) = \frac{54.47s^2 + 2.317s + 0.02446}{s^2 + 0.002033s + 4.374e-06},$$

and closed-loop stability is certified with algorithm 1.

As the last step the nonlinear crystallizer is simulated in closed loop with controller K^* .

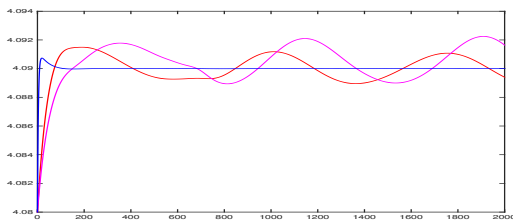


Figure 6. Simulation of K^* with nonlinear system. The system is steered from old steady-state $c_{ss} = 4.08$ to new steady-state at $c_{ss} = 4.09$. Time is in minutes.

The simulation uses a finite-difference semi-discretization with 4000 spatial steps. Blue shows controlled, red and magenta uncontrolled linearized and nonlinear state $c(t)$. The spatial resolution required for the desired precision is critical for a state-space control approach, and if state-space were used for control, system reduction would be inevitable.

7. Delay systems

Systems with delays are conveniently addressed by our novel synthesis technique. Semigroup theory is available [20], and the Nyquist test is applicable under hypotheses (iv), (v). Standard tests for stabilizability and detectability exist and resemble those for rational systems. In the following, we illustrate the efficiency of our method in four typical studies.

In the process industry, dead-time is a common phenomenon which may cause standard controllers to over-react to disturbances or set-point changes. The practical question is to decide whether or not dead-time is significant enough to be accounted for. One way to handle this is the celebrated Smith predictor [37] shown in Fig. 7. It applies to systems of the form $G(s) = G_0(s)e^{-\tau s}$, where τ is the delay, and where the delay-free $G_0(s)$ is called the lag. Typically, delay and lag are not precisely known, and we assume here for the purpose of illustration that a frequency sampled version $G(j\omega_v)$ of $G(s)$ is available for synthesis via (2). The Smith scenario now requires a model $G_m(s) = G_{m,0}(s)^{-\tau' s}$ of the process, where $G_{m,0}$ is an estimation of the lag, τ' an estimation of the delay.

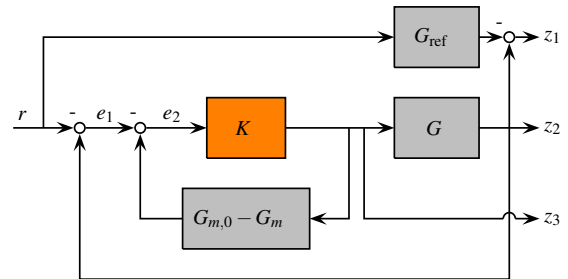


Figure 7. Synthesis interconnection with Smith predictor

Example 3. Lag dominant process. Our first delay study uses an example from [38], where it is assumed that the lag of G is correctly identified, while an inaccurate guess $\tau' = 5.0$ of the true dead time $\tau = 5.5$ is made:

$$G(s) := G_{m,0}(s)e^{-5.5s}, G_m(s) := G_{m,0}(s)e^{-5.0s}. \quad (23)$$

We assume that frequency samples $G(j\omega_v)$ of the dead-time system G are available on a grid Ω_{opt} , but that on demand further sampled values $G(j\omega)$ can be obtained. Dead-time-free and delay-free reference systems are

$$G_{m,0}(s) := \frac{1}{(1+5s)(1+10s)}, \quad G_{\text{ref},0}(s) = \frac{3}{3+10s}.$$

Since the time constant of the process exceeds the delay time, the process is *lag-dominant*. The purpose of the reference

model is to reduce the lag in closed loop, and it includes the incompressible model delay $\tau' = 5.0$, which leads to $G_{\text{ref}}(s) = G_{\text{ref},0}(s)e^{-\tau's}$.

The H_∞ -control problem minimizes the channel $r \rightarrow z = (z_1, z_2, z_3)$ with weight $W(s) = [w_1(s); w_2(s); w_3]$. Here T_{z_1r} reflects set-point tracking, with $w_1(s) = \frac{0.01s+0.5986}{s+0.005986}$ a low-pass filter with crossover frequency at twice the bandwidth of the reference model G_{ref} . The channel T_{z_2r} assesses mismatch between model G_m and system G on an appropriate frequency range described by the robustness weight $w_2(s) = \frac{2.39s+0.4078}{s+2.044}$, which is built as a tight upper bound of the relative uncertainty between the 3 models in (23). Finally, to limit the control effort the transfer function T_{z_3r} with weight $w_3 = 0.1$ is included in the objective. Problem (2) is now solved via algorithm 3, where primary controllers K are in the class \mathcal{K}_{pid} of SISO PIDs. The optimal controller

$$K^*(s) = 2.93 + \frac{0.207}{s} + \frac{9.46s}{1+1.64s}, \quad (24)$$

is obtained in 14s CPU using 33 iterations. It achieves good step responses, as seen in Fig. 8, and requires lower gain in the high frequency range compared to the loop-shaping controller given in [38], as seen in Fig. 9. K^* is competitive with other controllers proposed for this study in the literature [39, 40, 41, 42].

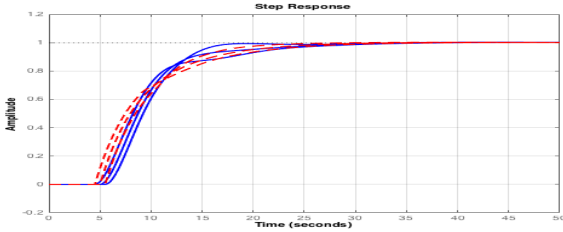


Figure 8. Step responses. Primary PID controller (24) (solid), controller in [38] (dotted)

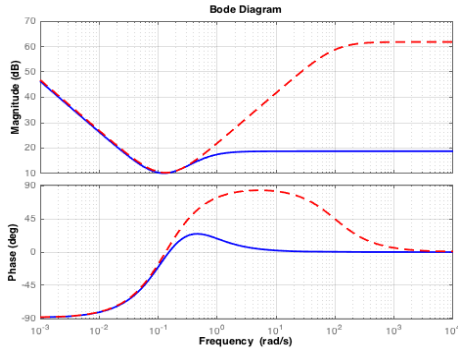


Figure 9. Bode plots. PID (solid), controller in [38] (dotted)

Example 4. Dead-time dominant process. Our second delay study is from [43] and follows again Fig. 7. With the

same notations

$$\begin{aligned} G(s) &= \frac{5.0}{1+38s}e^{-90s}, & G_m(s) &= \frac{5.6e^{-93.9s}}{1+40.2s}, \\ G_{\text{test}}(s) &= \frac{6}{1+42s}e^{-100s}, & G_{\text{ref}}(s) &= \frac{e^{-93.9s}}{1.33.33s} \end{aligned} \quad (25)$$

which due to the large delay is now *dead-time dominant*. Here G_{test} is used for posterior testing. Weighting filters are given as $w_3 = 0$ and

$$w_1(s) = \frac{5}{(20s+1)^2}, \quad w_2(s) = \frac{2.661s+0.04519}{s+0.2265}.$$

The primary controller is a PI, and algorithm 3 gives the optimal $K_1 = 0.141 + 0.00645/s$. Step responses are shown in Figure 10 and exhibit significant overshoots and undershoots, which are chief features of long time-delay systems.

The transient behavior can be improved if larger settling times are accepted. With the modified reference model $G_{\text{ref}} = e^{-93.9s}/(1+70s)$ better transients are obtained, as seen in Fig. 10. The new primary PI obtained with algorithm 2 is now $K_2 = 0.0729 + 0.00322/s$.

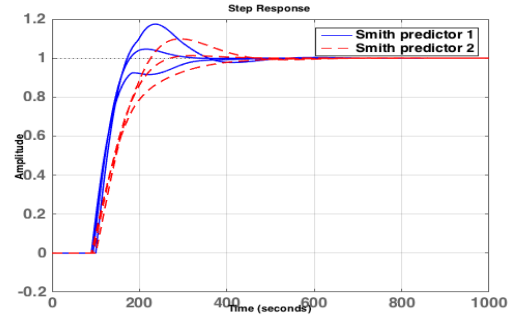


Figure 10. Step responses. PI primary controller K_1 (solid), PI primary controller K_2 (dashed)

Example 5. Cavity flow. A detailed study of cavity flows is given in [44, 45]. This challenging problem is taken from [46], where the infinite dimensional transfer function is available analytically as

$$G(s) = \frac{e^{-\tau_1 s}}{p_2(s) + q_2(s)e^{-\tau_2 s} + ce^{-\tau_3 s}},$$

with quadratic polynomials p_2, q_2 . The H_∞ -objective is

$$\|(W_1 S, W_2 T)\|_\infty,$$

where $W_1(s) = (0.01s + 502.5)/(s + 50.25)$, $W_2(s) = (100s + 500)/(s + 50000)$. Optimization is over the class \mathcal{K}_2 of order 2 controllers. The optimal $K^*(s) = (0.718s^2 + 224.7s + 2642)/(s^2 + 535.8s + 2.268e04)$ achieves a final gain of $\gamma^* = 5.41$. The final grid size is $|\Omega_{\text{opt}}| = 382$, no update was necessary. Note that this test case can be approached using `systeme` but requires a 15th-order Padé for the delay resulting in a 47th-order plant.

Example 6. Van de Vusse reactor [47]. An H_∞ problem for a heat exchanger was solved in [47], and here this model

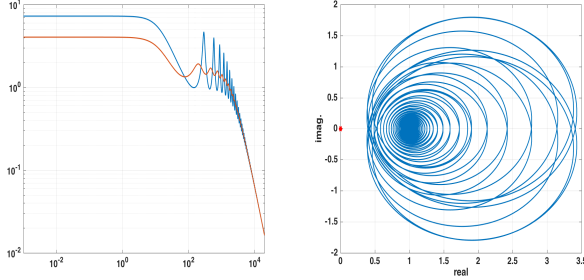


Figure 11. Cavity flow problem from [46]. Left image shows magnitude of $G(s)$ (blue) and GS in closed loop (red). Right image shows the final Nyquist curve for $\omega \in [-3e4, 3e4]$.

is applied to a Van de Vusse reactor. Weighting filters were chosen as $W_u = 0.1$,

$$W_e = \frac{10^{-5}s + 1.502}{s + 0.07509}, \quad W_n = \frac{0.00125s^2 + 0.00035s + 5 \cdot 10^{-5}}{2.5 \cdot 10^{-5}s^2 + 0.007s + 1},$$

where W_e and W_u penalize tracking error and control effort, respectively. The filter W_n specifies the frequency content of a noise input. While [47] considers full-order controllers of a suitable rational approximation, we use our transfer-function based approach in remark 10, where we restrict for practical reasons optimization to the class \mathcal{K}_3 of 3rd-order controllers. Algorithm 3 yields an optimal $K^* \in \mathcal{K}_3$ with state-space representation

$$\begin{bmatrix} -27.5666 & -26.2507 & 0 & 3.5532 \\ 21.9919 & -6.3124 & 2.9680 & 16.2390 \\ 0 & 0.6141 & -1.6018 & 2.2726 \\ 4.4793 & -2.3704 & 1.8102 & -0.0768 \end{bmatrix},$$

with certified locally optimal value $\gamma^* = 0.464$.

Examples 7. MIMO delay. We consider studies from [48] with MIMO processes $G(s)$ with multiple input/output delays $G_{ij}(s) = G_{ij}^0(s)e^{-\tau_{ij}s}$, where $G_{ij}^0(s)$ are rational. All systems are square with dimensions 2 to 4.

The control scheme is a mixed sensitivity problem as in figure 5. For G the first 2×2 study in [48] weightings are $W_e = w_e I_2$, $W_u = 0.01 I_2$, $W_y = w_y I_2$ and $w_e(s) = \frac{0.01s + 0.2512}{s + 0.02512}$, $w_y(s) = \frac{100s + 5}{s + 500}$. The final H_∞ -norm is $\gamma^* = 1.07$, and is certified using Lemma 4. The method ends with $|\Omega_{\text{opt}}| = 766$, for which it needs one update of the grid. The optimal $K^* \in \mathcal{K}_3$ was obtained as $[A_K \ B_K; C_K \ D_K] =$

$$\begin{bmatrix} -6.407 & 0.128 & 0 & -0.04964 & 3.273 \\ -1.189 & 0.006017 & -0.04487 & -0.5266 & 0.7091 \\ 0 & 0.02529 & -0.0794 & -0.439 & -0.2358 \\ -2.454 & -0.1121 & 0.1447 & 0.2772 & 1.092 \\ -27.94 & 0.6764 & -0.4109 & -0.1795 & 15.78 \end{bmatrix}.$$

When allowed random restarts, systune with order 3 Padé approximation gives the same H_∞ -norm. Results for the remaining 2×2 , 3×3 and 4×4 examples from [48] are collected in Table 3 and the details are available upon request.

8. Comparison with convex-concave procedure

In this section we compare our approach to the convex-concave procedure (CCP) of [12, 13, 11]. The example is taken from [13], with process G given as

$$G(s) = \begin{bmatrix} \frac{1}{s+1} & \frac{0.2}{s+3} & \frac{0.3}{s+0.5} \\ \frac{0.1}{s+2} & \frac{1}{s+1} & \frac{1}{s+1} \\ \frac{0.1}{s+0.5} & \frac{0.5}{s+2} & \frac{1}{s+1} \end{bmatrix}.$$

The problem is a standard mixed-sensitivity problem involving the weighted transfer functions $W_1 S$ and $W_2 K S$ with $W_1 := (s+3)/(3s+0.3)$ and $W_2 := (10s+2)/(s+40)$. The fine frequency grid Ω_{fine} covers the interval $[10^{-2}, 10^2]$ with $N = |\Omega_{\text{fine}}| = 1000$ points.

In [13], controllers are chosen as matrix fractions of polynomials $K(s) := N(s)D(s)^{-1}$, with

$$N(s) = N_d s^d + \dots + N_1 s + N_0, \quad D(s) = I_d s^d + \dots + D_1 s + D_0.$$

Formally these K have high order, but can be substantially reduced by taking minimal realization of order $\deg \det D(s)$. For instance, with $d = 3$ the fractional controller has order 27, but can be reduced to order 9. For comparison we compute controllers in state-space form (3) of increasing order $\text{size}(A_K)$ using our approach and stop when no further progress is observed. Results are summarized in Table 2. To evaluate our non-smooth approach, we also report execution times (column 4) and the number of frequencies $|\Omega_{\text{opt}}|$ that were used (column 5).

Table 2. Comparison of CCP procedure with trust-region non-smooth technique

K order	γ^* CCP	γ^* non-smooth	cpu time (sec.)	$ \Omega_{\text{opt}} $
1	na*	6.27	4.47	106
2	na	5.14	6.39	106
3	1.52	1.42	12.85	106
4	na	1.22	10.57	106
5	na	1.22	12.19	106
6	1.25	1.21	10.17	106
7	na			
8	na			
9	1.22			
15	1.21			

na: non available

Both techniques give comparable results. Our approach reaches the globally optimal value $\gamma^* = 1.21$ for a lower-order controller, taking advantage of working with state-space representations (3). Also, our algorithm uses a fairly small number of frequencies for both stability and performance, showing that sampling at higher densities is unnecessary. State-space data of the 4th-order optimal controller with certified $\gamma^* = 1.22$ is given as:

$$\begin{bmatrix} -1.1297 & 2.4687 & 0 & 0 & -0.62558 & 2.1069 & 2.4133 \\ 0.49873 & -1.7456 & -0.0056164 & 0 & -0.34424 & 1.25 & 0.07677 \\ 0 & 0.23265 & -0.034507 & -0.17205 & -0.78512 & -2.9273 & 1.2731 \\ 0 & 0 & 0.047156 & -0.24021 & -0.86441 & -0.76551 & 0.29947 \\ -0.2634 & -0.17576 & 0.41289 & -2.1632 & 0.11309 & -0.016873 & -0.01568 \\ -0.8761 & 2.5224 & -0.64724 & 0.59545 & 0.0138 & 0.11148 & -0.0338 \\ 1.0477 & -1.3105 & 0.43259 & -0.22984 & 0.0107 & 0.03145 & 0.098511 \end{bmatrix}.$$

9. More exhaustive testing

Our method was tested on a bench of 40 plants, where algorithm 3 could be crosschecked. Table 3 shows examples from the Compleib collection [19], identified by their acronyms in column 1. As these examples (1-28) are finite dimensional, `sysune` based on [1, 49] was used to compare with a standard structured H_∞ -synthesis [1]. For these tests the controller structure \mathcal{K}_6 of 6th-order controllers was used. Column 'algo. 3' gives the result of algorithm 3, with $|\Omega_{\text{opt}}|$ the size of the grid on exit, where column 'updates' gives the number of restarts in step 4 of algorithm 3. For instance, in study 'MFP' our method computed $K^* \in \mathcal{K}_6$ with optimal gain $\gamma^* = 4.27$ certified on exit. That is, $\|T_{wz}(P, K^*)\|_\infty = 4.27 + \vartheta$ with $|\vartheta| < 10^{-2}$. This was obtained with $|\Omega_{\text{opt}}| = 80$ and required 1 updating. Running `sysune` on the same example gave K_{sys} with the same structure and slightly better gain $\gamma_{\text{sys}} = 4.20$.

test	sysune	algo. 3	$ \Omega_{\text{opt}} $	updates
AC3	3.10	2.98	2115	1
AC6	3.52	3.65	108	1
AC15	14.87	14.93	82	1
AC16	14.86	14.87	90	1
AC17	6.61	6.61	44	1
HE2	2.45	2.45	112	2
DIS1	4.16	4.17	105	1
DIS3	1.04	1.05	185	1
TG1	3.47	3.47	243	1
AGS	8.17	8.17	92	1
WEC2	3.60	3.60	272	1
WEC3	3.77	3.77	283	1
BDT1	0.27	0.27	37	1
MFP	4.20	4.27	80	1
UWV	0.00	0.00	582	2
EB1	3.09	3.10	140	2
EB2	1.77	1.78	198	1
PSM	0.92	0.92	89	1
NN4	1.29	1.29	118	1
NN8	2.36	2.36	58	1
NN11	0.0155	0.0255	138	1
HF2D12	1037666.47	1037666.23	89	1
HF2D13	101548.53	101548.54	211	1
CM1	0.82	0.82	136	1
DLR1	0.07	0.07	119	1
JE1	4.14	4.15	958	1
DLR2	201.28	147.22	6203	6
DLR3	382.51	504.37	3546	7
heat-N	—	0.39	26	0
heat-D	—	0.60	17	1
heat-M	—	0.66	11	0
reactor [47]	—	0.46	101	1
beam [50]	0.14[50]	0.14	201	1
state-delay [51]	0.2019	0.2015	81	0
MIMO delay1 [48]	1.07	1.07	766	1
MIMO delay2 [48]	1.61	1.61	260	1
MIMO delay3 [48]	1.59	1.48	195	0
MIMO delay4 [48]	0.47	0.51	2387	2
cavity [46]	5.55	5.41	382	0
crystallizer	—	1.18	550	0

Table 3. Test bench with 28 CompLeib examples and 12 infinite-dimensional studies

The 12 infinite-dimensional examples in Table 3 include in particular the studies heat-N, heat-D, heat-M, which use example 1 with Neumann, Dirichlet and mixed boundary conditions, where optimization is over the class \mathcal{K}_1 of first-order controllers. The H_∞ -controllers are $K_N(s) = (1.318s - 45.64)/(s + 4.493)$, $K_D(s) = (1.602s + 14.05)/(s + 0.2962)$, $K_M(s) = (5.885s + 12.31)/(s + 0.2916)$. In all heat studies the weights $W_e(s) = (0.01s + 3.015)/(s + 0.3015)$, $W_u = 0.01$ and $W_y(s) = (100s + 10)/(s + 1000)$ were used. The goal of each design was to track the set-point temperature at $\xi_0 = 1/3$, and to attenuate high frequency measurement noise.

The state-delay study uses a system with 2 states and state delay from [51]. The weights are $W_e(s) = (0.001s + 5.244)/(s + 0.5244)$, $W_u(s) = W_y(s) = (100s + 1.5)/(s + 1500)$, the channel is $r \rightarrow (W_e e, W_u u, W_y y)$. Here, e denotes the tracking error with a reference model $\frac{3^2}{s^2 + 2 \times 0.8 \times 3s + 3^2}$. The optimal 2nd-order 2-DOF controller obtained by algorithm 3 is $K^*(s) = [0.9032s^2 + 7.546s + 9.488, -0.9052s^2 - 6.869s + 3.803]/(s^2 + 0.9293s + 6.63)$. As before, this result is certified with $\vartheta = 1\text{e-}2$ absolute accuracy, and crosschecked by `sysune` with a 4th-order Padé approximation of the delay.

10. Conclusion

In this paper, we have presented a novel method for the synthesis of structured LTI controllers for a large class of infinite-dimensional systems described by their frequency response. Our method leverages non-smooth optimization techniques to compute locally optimal H_∞ -controllers.

Several frequency sampling techniques have been studied and a new adaptive sampling method for synthesis has been derived, which allows to certify exponential stability in closed loop and to compute H_∞ -performance of the resulting controllers within a fixed tolerance level ϑ .

Our method is applicable to a fairly broad class of infinite-dimensional systems, including delay and integral-differential equations, boundary and distributed control of PDEs, and systems described by frequency-domain data. Local optimality certificates for program (2) are provided, and numerical testing confirms the excellent performance of the method, which often finds global optima. The method was evaluated on a large test bench including linearized PDEs, state-delayed and MIMO dead-time systems, and more detailed studies in process control.

References

- [1] P. Apkarian and D. Noll. Nonsmooth H_∞ synthesis. *IEEE Trans. Automat. Control*, 51(1):71–86, January 2006.
- [2] R. Hettich and K. O. Kortanek. Semi-infinite programming: theory, methods, and applications. *SIAM Review*, 35:380–429, 1993.
- [3] S. Boyd and V. Balakrishnan. A regularity result for the singular values of a transfer matrix and a quadratically convergent algorithm for computing its \mathbf{L}_∞ -norm. *Syst. Control Letters*, 15:1–7, 1990.
- [4] P. Apkarian, D. Noll, and L. Ravanbod. Nonsmooth bundle trust-region algorithm with applications to robust stability. *Set-Valued and Variational Analysis*, 24(1):115–148, 2016.
- [5] P. Apkarian, D. Noll, and L. Ravanbod. Computing the structured distance to instability. In *SIAM Conference on Control and its Applications*, pages 423–430, 2015.

- [6] E. Polak and Y. Wardi. A nondifferentiable optimization algorithm for the design of control systems subject to singular value inequalities over a frequency range. *Automatica*, 18(3):267–283, 1982.
- [7] I. Horowitz. Quantitative feedback theory. *IEE Proc.*, 129-D(6):215–226, November 1982.
- [8] E. van Solingen, J.W. van Wingerden, and T. Oomen. Frequency-domain optimization of fixed-structure controllers. *International Journal of Robust and Nonlinear Control*, 2016.
- [9] Gorka Galdos, Alireza Karimi, and Roland Longchamp. H_∞ controller design for spectral mimo models by convex optimization. *Journal of Process Control*, 20(10):1175–1182, 2010.
- [10] A. Karimi, M. Kunze, and R. Longchamp. Robust PID controller design by linear programming. In *2006 American Control Conference*, pages 3931–3836, June 2006.
- [11] M. Hast, K. J. Aström, B. Bernhardsson, and S. Boyd. PID design by convex-concave optimization. In *2013 European Control Conference (ECC)*, pages 4460–4465, July 2013.
- [12] S. Boyd, M. Hast, and K.J. Aström. MIMO PID tuning via iterated LMI restriction. *International Journal of Robust and Nonlinear Control*, 26(8):1718–1731, 2016. rnc.3376.
- [13] A Karimi and C Kammer. A data-driven approach to robust control of multivariable systems by convex optimization. *arXiv:1610.08776*, 2016.
- [14] Thomas Lipp and Stephen Boyd. Variations and extension of the convex–concave procedure. *Optimization and Engineering*, 17(2):263–287, Jun 2016.
- [15] H. Logemann. On the Nyquist criterion and robust stabilization for infinite-dimensional systems. In M. A. Kaashoek, J. H. van Schuppen, and A. C. M Ran, editors, *Robust Control of Linear Systems and Nonlinear Control: Proceedings of the International Symposium MTNS-89, Volume II*, pages 627–634. Birkhäuser Boston, Boston, MA, 1990.
- [16] A. Sasane. An abstract Nyquist criterion containing old and new results. *Journal of Mathematical Analysis and Applications*, 370(2):703 – 715, 2010.
- [17] M. Fardad and B. Bamieh. An extension of the argument principle and Nyquist criterion to a class of systems with unbounded generators. *IEEE Trans. Aut. Control*, 53(1):379–384, 2008.
- [18] R. Curtain. A synthesis of time and frequency domain methods for the control of infinite-dimensional systems: A system theoretic approach. *SIAM Frontiers in Applied Mathematics*, 1989.
- [19] F. Leibfritz. COMPLIB, CONstraint Matrix-optimization Problem Library - a collection of test examples for nonlinear semidefinite programs, control system design and related problems. Technical report, Universität Trier, 2003.
- [20] R. F. Curtain and H. Zwart. *An Introduction to Infinite-Dimensional Linear Systems Theory*, volume 21 of *Texts in Applied Mathematics*. Springer-Verlag, 1995.
- [21] K.-J. Engel and R. Nagel. *One-Parameter Semigroups for Linear Evolution Equations*. Springer Graduate Texts in Math. Springer, 2000.
- [22] C.A. Jacobson and C.N. Nett. Linear state-space systems in infinite-dimensional space: the role and characterization of joint stabilizability/detectability. *IEEE Trans. Aut. Control*, 33:541–549, 1988.
- [23] Hsiao-Ping Huang, Chung-Tarng Jiang, and Yung-Chen Chao. A new Nyquist test for the stability of control systems. *International Journal of Control*, 58(1):97–112, 1993.
- [24] P. Apkarian and D. Noll. Nonsmooth optimization for multidisk H_∞ synthesis. *European J. of Control*, 12(3):229–244, 2006.
- [25] J.V. Burke, A.S. Lewis, and M.L. Overton. Two numerical methods for optimizing matrix stability. *Linear Algebra and its Applications* 351-352, pages 147–184, 2002.
- [26] V. Bompert, P. Apkarian, and D. Noll. Nonsmooth techniques for stabilizing linear systems. In *Proc. American Control Conf.*, pages 1245–1250, New York, NY, July 2007.
- [27] T. Kato. *Perturbation theory for linear operators; 2nd ed.* Grundlehren Math. Wiss. Springer, Berlin, 1976.
- [28] S. Mossaheb. On the existence of right-coprime factorization for functions meromorphic in a half-plane. *IEEE Transactions on Automatic Control*, 25(3):550–551, Jun 1980.
- [29] O. J. Staffans. Coprime factorizations and well-posed linear systems. *SIAM J. Control and Optimization*, 36(4):1268–1292, 1998.
- [30] D. Salamon. Infinite dimensional linear systems with unbounded control and observation: a functional analytic approach. *Transactions of the American Mathematical Society*, 300(2):383–431, 1987.
- [31] R. Curtain and K. Morris. Transfer functions of distributed parameter systems: A tutorial. *Automatica*, 45(5):1101 – 1116, 2009.
- [32] M. Renardy. On the linear stability of hyperbolic PDEs and viscoelastic flows. *Zeitschrift für angewandte Mathematik und Physik ZAMP*, 45(6):854–865, 1994.
- [33] M. Lichtner. Spectral mapping theorem for linear hyperbolic systems. *Proc. Amer. Math. Soc.*, 136(6):2091–2101, 2008.
- [34] H. Zwart. Linearization and exponential stability. *arXiv:1404.3475v1*, 2014.

- [35] U. Vollmer and J. Raisch. H_∞ -control of a continuous crystallizer. *Control Engineering Practice*, 9:837–845, 2001.
- [36] A. Rachah, D. Noll, F. Espitalier, and F. Baillon. A mathematical model for continuous crystallization. *Mathematical Methods in the Applied Sciences*, 39(5):1101–1120, 2016.
- [37] O. J. M. Smith. Closer control of loops with dead time. *Chemical Engineering Progress*, 53(9):217–219, 1957.
- [38] Vinicius de Oliveira and Alireza Karimi. Robust Smith predictor design for time-delay systems with H_∞ performance. *IFAC Proceedings Volumes*, 46(3):102 – 107, 2013.
- [39] I. Kaya. Tuning Smith predictors using simple formulas derived from optimal responses. *Industrial & Engineering Chemistry Research*, 40(12):2654–2659, 2001.
- [40] Z. J. Palmor and M. Blau. An auto-tuner for Smith dead time compensator. *Int. Journal of Control*, 60(1):117–135, 1994.
- [41] T. Hagglund. A predictive PI controller for processes with long dead times. *IEEE Control Systems*, 12(1):57–60, Feb 1992.
- [42] Chang-Chieh Hang, Qingguo Wang, and Li-Sheng Cao. Self-tuning Smith predictors for processes with long dead time. *International Journal of Adaptive Control and Signal Processing*, 9(3):255–270, 1995.
- [43] P. Gahinet and L. F. Shampine. Software for modeling and analysis of linear systems with delays. In *Proc. American Control Conf.*, volume 6, pages 5600–5605, June 2004.
- [44] P. Yan, M. Debiasi, X. Yuan, J. Little, H. Özbay, and M. Samimy. Experimental study of linear closed-loop control of subsonic cavity flow. *AIAA Journal*, 44(5):929–938, 2006.
- [45] P. Yan, X. Yuan, H. Ozbay, M. Debiasi, E. Caraballo, M. Samimy, J. M. Myatt, and A. Serrani. Modeling and feedback control for subsonic cavity flows: A collaborative approach. In *Proceedings of the 44th IEEE Conference on Decision and Control*, pages 5492–5497, Dec 2005.
- [46] Xin Yuan, Mehmet Önder Efe, and Hitay Özbay. On delay-based linear models and robust control of cavity flows. In Silviu-Iulian Niculescu and Keqin Gu, editors, *Advances in Time-Delay Systems*, pages 287–298. Springer Berlin Heidelberg, Berlin, Heidelberg, 2004.
- [47] H. Sano. H_∞ -control of a parallel-flow heat exchange process. *Bulletin of the Polish Academy of Sciences*, 65(1):11–19, 2017.
- [48] Qiang Xiong and Wen-Jian Cai. Effective transfer function method for decentralized control system design of multi-input multi-output processes. *Journal of Process Control*, 16(8):773 – 784, 2006.
- [49] P. Apkarian, P. Gahinet, and C. Buhr. Multi-model, multi-objective tuning of fixed-structure controllers. In *European Control Conference (ECC)*, pages 856–861. IEEE, 2014.
- [50] C. Foias, Hitay Özbay, and Allen R. Tannenbaum. *Robust Control of Infinite Dimensional Systems: Frequency Domain Methods*. Springer-Verlag New York, Inc., Secaucus, NJ, USA, 1996.
- [51] M. Park, O. Kwon, J. Park, and S. Lee. Delay-dependent stability criteria for linear time-delay system of neutral type. *International Journal of Computer, Electrical, Automation, Control and Information Engineering*, 4(10):1602–1606, 2010.